Journal of Low Temperature Physics, Vol. 110, Nos. 5/6, 1998

The Superfluid ^{4}He Analog of the RF SQUID

K. Schwab, N. Bruckner, and Richard Packard

Physics Department, University of California, Berkeley, California 94720, USA

(Received July 3, 1997; revised October 29, 1997)

We describe the theory, design, fabrication, and performance of a superfluid ^{4}He device which is the analog of the superconducting RF SQUID. This device is a sensitive rotation detector and is used to sense the rotation of the Earth. We also describe the experimental developments and observations which lead to the construction of this successful device.

I. INTRODUCTION

This paper describes a superfluid analog of the superconducting RF SQUID.[1] Whereas an RF SQUID is sensitive to magnetic flux, the ^{4}He SQUID (Superfluid QUantum Interference Device) is sensitive to absolute rotation. The device described here exhibits several of the characteristic phenomena of SQUIDs. For example: There is a "staircase" response function. The slope of the staircase response is determined by the fluctuation phenomena underlying phase slips in a weak link. The device performance is sensitive to the uncontrolled motion of quantized vortices. Performance is adversely affected by the excitation of normal modes of the device. Fundamental fluctuations, thermal in this case, determine the noise floor of the device.

The theory describing the ^{4}He SQUID rests on the very foundation of the theory of superfluidity in ^{4}He.[2] The state of superfluid ^{4}He is described by a macroscopic wave function whose phase, ϕ, is proportional to the superfluid velocity potential:

$$\vec{v}_s = \frac{h}{m_4} \nabla \phi \tag{1.1}$$

Here h is Planck's constant divided by 2π and m_4 is the atomic mass of ^{4}He. If the wavefunction is to be single valued, the phase can advance

0022-2291/98/0300-1043$15.00/0

around a contour only by integer values of 2π. This implies that the circulation is quantized:

$$\oint \vec{v}_s \cdot \vec{dl} = n\frac{h}{m_4}, \qquad n = 0, \pm 1, \pm 2, \ldots \tag{1.2}$$

Thus the accessible flow states are limited to a discrete set. In a multiply connected topology (e.g., a toroidal container) flow is quantized about irreducible paths. In a simply connected container, rotation of the fluid is accomplished by a distribution of singly quantized vortex lines. In this way the quantum fluid attempts to approximate the solid body rotation of a classical fluid. For small rotation speeds in a cylindrically symmetric container, the superfluid remains in the $n = 0$ quantization state and remains stationary with respect to an absolute inertial frame.

For over 25 years it has been recognized that in principle, absolute rotation could be detected using a device which relies on the superfluid's property of quantized circulation, and which is closely analogous to the superconducting RF SQUID. Experiments aimed at constructing such an analog fall into three types and before this year, have had only limited success: torsional oscillators,[3-6] Helmholtz oscillators,[7] and diaphragm-aperture (D-A) oscillators.[8-10] Due to recent advances which allow the detection of single phase slips (see below) in concert with the development of microfabrication techniques, the stage has been set to exploit the quantization of circulation to demonstrate a superfluid detector of absolute rotation. Our group in Berkeley[11] as well as a group in France[12, 13] have successfully used the ^{4}He SQUID to detect the Earth's rotation.

Motivations for constructing sensitive superfluid gyroscopes are found from widely varied sources, such as the geodesy community, and physicist interested in experimental general relativity. The Earth's rotation possesses fluctuations on the order of 10^{-12}–10^{-13} rads/sec with measurement periods of many hours to many days.[14] Also, it has been proposed[15, 16, 5, 17] that a high sensitivity superfluid gyroscope might be used to measure general relativistic effects such as gravitational radiation and the Lense–Thirring effect.[18] Gyroscopes intended to detect these signals are proposed to be quite large (400 m of tubing, coiled 127 turns about a radius of 0.5 m), with measurement times of ~ 1 year. These signals will require a much higher sensitivity gyroscope than what has been demonstrated in Berkeley or in France (a factor of 10^4 improvement to resolve the fluctuations in the Earth's rotation, and a factor of 10^6 for the Lense–Thirring effect). What has been shown, is the first proof of principle which may ultimately lead to these extreme levels of rotation sensitivity in the future and rival the best existing gyroscopes.[19]

This paper is organized as follows. We begin by describing the fundamental principles of the ^{4}He SQUID. Section II describes how superfluid couples to rotation. In Sec. III, we describe the theory of quantized dissipation in superflow through apertures followed by the theory of D-A oscillators used to detect the dissipation and the effects of rotation in Sec. IV. Section V details the physical conditions necessary for successful device operation.

Section VI discusses the limits of the rotation sensitivity. In Sec. VII, we describe the design and construction of two D-A oscillators followed by the experimental performance in Sec. VIII. Our conclusions are in Sec. IX. Finally, we give two appendixes describing the details of the superfluid flow fields, Appendix A, and the fabrication procedure used to produce our D-A oscillators, Appendix B.

II. ROTATING SUPERFLOW

To understand how rotation can lead to measurable changes in the properties of superfluids, it is necessary to understand the behavior of superfluids in rotating containers. The derived effects rest on the fundamental properties of superflow, that is, curl-free motion and quantization of circulation. The simplest superfluid container which demonstrates the basic coupling to rotation is a toroidal container. We will first consider this topology. This ideal situation is closely realized in the ongoing torsional-oscillator experiments in Trento, Italy[20] and we will use their particular geometry as an example for the numerical calculations.[21]

Consider a right, annular container of inner radius R_{in}, outer radius R_{out}, height H, and with a solid septum (no aperture). A cross-section through such a container is shown in Fig. 1. The container rotates with angular velocity $\vec{\omega} = \omega \hat{z}$ about the axis of the annulus, $\hat{z}$. The calculation of the velocity field simplifies to a two dimensional flow problem since the superfluid flow field will have no $\hat{z}$ dependence. To calculate the superfluid velocity throughout the container, we can first solve for the velocity potential (the quantum phase) and take the gradient everywhere to compute the velocity field. This is preferable since under the assumption that the superfluid is incompressible, the superflow is divergence free and thus the quantum phase satisfies Laplace's equation:

$$\nabla \cdot \vec{v} = 0 \rightarrow \nabla^2 \phi = 0 \tag{2.1}$$

Numerical techniques to solve Laplace's equation are straight-forward and readily available. Along the inner and outer cylindrical walls, the boundary

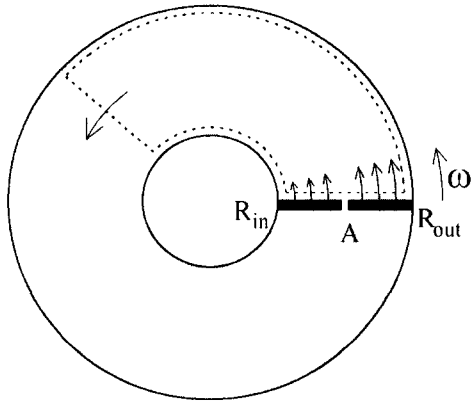

Fig. 1. Rotating annular container of superfluid with septum. Dotted line is Gaussian surface used below and in Appendix A.

condition is $\nabla\phi \cdot \hat{n} = 0$. At the septum, the boundary condition is $\nabla\phi \cdot \hat{n} = (2\pi/\kappa_o)\,\omega r$, where $\kappa_o = h/m_4$. Using these conditions and a finite element analysis software package[22] we calculate the superfluid phase in the container. By taking the gradient of this phase, we find the superfluid velocity field.

Figure 2 shows the calculated phase in an annulus rotating with unit angular velocity. Figure 3 shows the velocity field in the rotating frame. One can see from the velocity field in the rotating frame, that along a contour approximately midway between R_{in} and R_{out}, the velocity is essentially zero. Therefore, in the inertial frame the superfluid is moving with velocity $\vec{v}_s = \omega r\hat{\theta}$ along this particular contour. However, the entire flow field is not solid body motion; for smaller radial positions the superfluid is moving faster than air, and for larger radial positions, the superfluid moves slower than ωr. (See Appendix A for a discussion of the superfluid flow field.)

Most importantly, one can see that a phase difference, $\Delta\phi_{\text{rot}}$, is developed across the septum when the container is rotated. Since

$$\Delta\phi = \frac{2\pi}{\kappa_o} \int \vec{v}_s \cdot \vec{dl} \tag{2.2}$$

we find by integrating around the annulus along the contour with $v_s = \omega r$, that this phase difference is:

$$\Delta\phi_{\text{rot}} = \frac{4\pi^2 \omega \bar{R}^2}{\kappa_o} = 2\pi \frac{2\omega \cdot \pi \bar{R}^2}{\kappa_o} \tag{2.3}$$

This relationship is of fundamental importance to the physics of a superfluid gyroscope and is verified in the numerical calculation shown in Fig. 2.

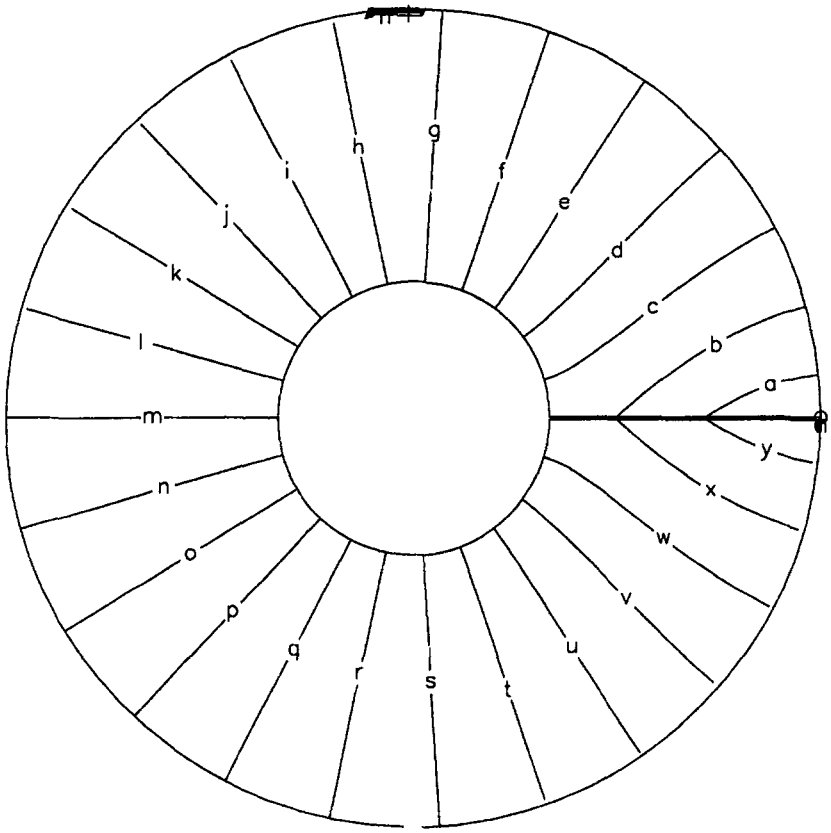

Fig. 2. Numerically calculated phase contours in a rotating annular container, where the dimensions are that of the Trento annulus and $\omega = 1$ rad/sec counter-clockwise. Contours increase counter-clockwise by steps of 1000 rads.

By casting the equation into the form on the right-hand side of Eq. (2.3), we can interpret the phase to be produced as a result of the application of a fictitious circulation "flux," $\Gamma = 2\omega\pi\bar{R}^2$, which is the product of a rotational "field", 2ω, and a sensing area $\pi\bar{R}^2$.

To provide an example of the size of the rotational coupling we set $\omega = \omega_{\text{earth}} = 72.9\ \mu(\text{rads/sec})$ and compute what value of R is necessary such that $\Gamma = \kappa_o$, (as will be shown in Sec. IV, the detectable changes induced in the superfluid from the applied circulation are periodic in the circulation constant κ_o),

$$R = \sqrt{\frac{\kappa_o}{2\pi\omega_{\text{earth}}}} = 1.5\ \text{cm} \tag{2.4}$$

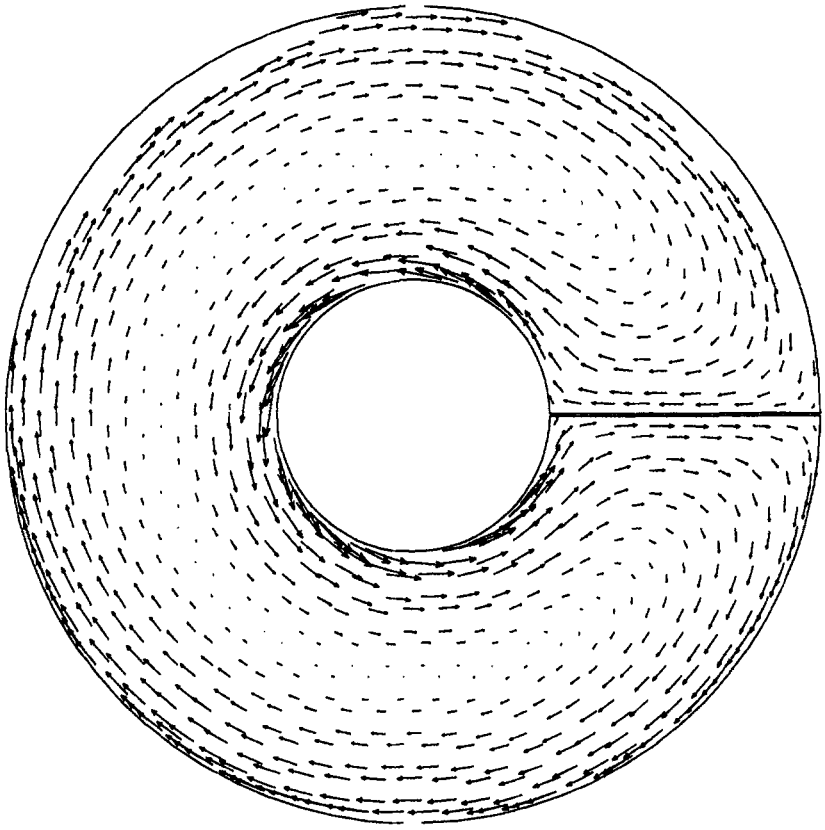

Fig. 3. Numerically calculated velocity field in the rotating frame.

One must devise a technique which makes this phase difference detectable. As will be shown, a small aperture placed in the septum will reveal this phase difference.

Suppose a small aperture is placed in the septum (small is quantified in Appendix A), with area a and hydrodynamic length l_a.[23] With the addition of the aperture comes a change in the topology of the container and the requirement that the circulation is quantized around this new irreducible path. The circulation integral contains two terms: one from the path around the annulus, and the other from the short path through the aperture. Specifically, if we integrate along the contour where $\vec{v}_s = \omega r \hat{\theta}$:

$$\oint \vec{v}_s \cdot \vec{dl} = \int_{\text{annulus}} \vec{v}_s \cdot \vec{dl} + \int_{\text{aperture}} \vec{v}_s \cdot \vec{dl} = \omega \bar{R} \cdot 2\pi \bar{R} + v_{\text{rot}} l_a = n\kappa_o \tag{2.5}$$

$$v_{\text{rot}} = n\frac{\kappa_o}{l_a} - \omega\bar{R}\cdot\frac{2\pi\bar{R}}{l_a} \tag{2.6}$$

Thus a current opposed to the direction of rotation is generated through the aperture. For example, if we start the annulus from rest, in the $n=0$ circulation state, and then begin to rotate, a current opposed to the direction of rotation is generated in the aperture such that the circulation state of the annulus remains fixed in the $n=0$ circulation state:

$$v_{\text{rot}} = -\omega\bar{R}\cdot\frac{2\pi\bar{R}}{l_a} \tag{2.7}$$

This current essentially "shields" the annulus from the applied circulation $2\omega\pi\bar{R}^2$. This behavior is analogous to the Meissner effect in superconductors, where a superconducting ring expels an applied magnetic flux by generating the appropriate supercurrents. The superfluid velocity induced in the hole, v_{rot}, is $(2\pi\bar{R}/l_a)$ times greater than $\omega\bar{R}$. This amplification of the rotational velocity can be quite large since $2\pi\bar{R}$ is macroscopic, while l_a can be made microscopic. For the torus in Trento with a 0.4 μm diameter orifice, this factor is $(2\pi\bar{R}/l_a) = 1.6\cdot 10^5$. The annulus and aperture act as a velocity amplifier, where the gain is determined by the ratio of the macroscopic circumference to microscopic hydrodynamic length.

The back-flow through the aperture, v_{rot}, can also be understood by considering the hydrodynamics of the spin-up of the annulus from rest. This will be helpful when we consider the limits on the time response of a superfluid gyroscope in Sec. V. It will be a useful for this analysis to define the concept of hydrodynamic inductance. Consider a tube of length l and of constant cross sectional area a, through which a fluid with density ρ, flows with velocity v. The energy E that is stored in the kinetic energy of flow is:

$$E = \frac{1}{2}\rho a l v_s^2 = \frac{1}{2}\frac{l}{\rho a}(\rho a v_s)^2 \equiv \frac{1}{2}LI^2 \tag{2.8}$$

where $I = \rho a v_s$ is the superfluid mass current, and $L \equiv (l/\rho a)$ defines the hydrodynamic inductance. For a tube that acts as a superleak, such as a sub-micron aperture, one uses ρ_s as the density instead of ρ. Using $v_s = (\kappa_o/2\pi)\nabla\phi$ we can calculate the quantum mechanical phase difference from one end of the tube to the other:

$$\Delta\phi = \frac{2\pi}{\kappa_o}LI \tag{2.9}$$

where $I = \rho_s a v_s$ is the super component of mass flow, and $L = (l/\rho_s a)$ is the hydrodynamic inductance for the superflow.

Finally, one can show that the relationship between the rate of change of the superfluid mass current, (dI/dt), in response to an applied hydrostatic pressure difference, Δp is:

$$\frac{1}{\rho}\Delta p = L\frac{dI}{dt} \tag{2.10}$$

This result follows from the Euler equation of motion for the superfluid and the assumption that the temperature is sufficiently low that thermomechanical pressures are negligable.[2]

Suppose the angular velocity of the annulus follows

$$\omega(t) = \begin{cases} 0 & -\infty < t \leqslant 0 \\ \omega_o \dfrac{t}{T} & 0 < t \leqslant T \\ \omega_o & T < t \leqslant +\infty \end{cases} \tag{2.11}$$

Assuming that the fluid is incompressible, the superfluid mass current in the bulk of the container must follow this motion: $I_{an} = \rho\sigma v_s = \rho\sigma\omega(t)\,\bar{R}$, where σ is the cross sectional area of the annulus, $\sigma = H\,\Delta R$. As the container spins-up, the acceleration of the supercurrent is:

$$\frac{dI_{an}}{dt} = \rho\sigma\frac{\omega_o}{T}\bar{R} \tag{2.12}$$

Using Eq. (2.10), we can calculate the pressure Δp generated across the septum which is necessary to accelerate the fluid at this rate, Eq. (2.12):

$$\Delta p = \rho L_{an}\frac{dI_{an}}{dt} = \rho 2\pi\bar{R}^2\frac{\omega_o}{T} \tag{2.13}$$

where $L_{an} \approx (2\pi\bar{R}/\rho H\,\Delta R)$. This pressure difference across the septum accelerates the fluid through the aperture. Again using Eq. (2.10), we can calculate the acceleration of the mass current through the aperture as a result of this pressure:

$$\frac{dI_a}{dt} = \frac{\Delta p}{\rho L_a} = \frac{L_{an}}{L_a}\frac{dI_{an}}{dt} = 2\pi\bar{R}^2\frac{\omega_o}{L_a T} = \rho_s a_s\left(\frac{2\pi\bar{R}}{l_s}\cdot\omega_o\bar{R}\right)\frac{1}{T} \tag{2.14}$$

After the time T, the velocity in the aperture will be $(2\pi\bar{R}/l_s)\cdot\omega_o\bar{R}$ which agrees with our previous calculation. One can see that the pressure generated by the inertia of the fluid in the bulk of the annulus is responsible for generating the back-flow through the aperture.

Using these relationships, it is possible to calculate the effect on the rotationally induced phase difference $\Delta\phi_{\text{rot}}$ as a result of the finite current that travels through the aperture. This will constrain the size of the aperture, or more precisely, the ratio of the hydrodynamic inductance of the aperture to the hydrodynamic inductance of the annulus.

First, by integrating Eq. (2.14) we find the familiar relationship for current division between ideal inductors:

$$I_a = \frac{L_{an}}{L_a}\cdot I_{an} \tag{2.15}$$

The mass current through the aperture is (L_{an}/L_a) times the mass current circulating in the bulk of the annulus. Then, let us create a Gaussian surface as shown in Fig. 1. We will add the contribution from mass current through the aperture, thus providing three sources of current through the Gaussian surface: the boundary condition at the rotating septum, the mass current in the bulk of the annulus, and the mass current through the aperture:

$$\begin{aligned}\int_S \vec{v}_s\cdot\vec{da} = 0 &= H\cdot\int_{\text{sept}}\omega r\,dr - H\int_{\text{bulk}}\vec{v}_s\cdot\hat{\theta}\,dr - \int_{\text{aperture}}\vec{v}_s\cdot\vec{da}\\ &= I_{\text{sept}} - I_{an} - I_a\end{aligned} \tag{2.16}$$

where the septum contribution is the mass current $I_{\text{sept}} = \rho(H\Delta R)\,\omega\bar{R}$. Using Eq. (2.15) to eliminate I_{an}, the mass current through the aperture is:

$$I_a = \frac{I_{\text{sept}}}{1+(L_a/L_{an})} \tag{2.17}$$

Using the relationship between mass current and phase difference, Eq. (2.9), we find that the phase across the aperture, produced by the mass current I_a, is:

$$\begin{aligned}\Delta\phi_{\text{rot}} &= \frac{2\pi}{\kappa_o}\left(\frac{L_a}{L_a+L_{an}}\right)L_{an}I_{\text{sept}}\\ &= \frac{4\pi^2}{\kappa_o}\omega\bar{R}^2\left(\frac{L_a}{L_a+L_{an}}\right) = \frac{4\pi^2}{\kappa_o}\omega\bar{R}^2\frac{\mathscr{R}}{(1+\mathscr{R})}\end{aligned} \tag{2.18}$$

where $\mathscr{R} \equiv (L_a/L_{an})$. One can see that for $L_a \gg L_{an}$, $\Delta\phi_{\rm rot}$ agrees with Eq. (2.3), where we ignored all contributions of the aperture. However, if $L_a \ll L_{an}$ then the phase across the aperture is reduced to:

$$\Delta\phi_{\rm rot} = \frac{4\pi^2}{\kappa_o} \omega \bar{R}^2 \frac{L_a}{L_{an}} \tag{2.19}$$

In the extreme limit where there is no septum, $L_a = 0$, and thus $\Delta\phi_{\rm rot} = 0$ since the superfluid remains stationary as the cylindrical walls slip by.

Equation 2.18 can be cast into another form once we recognize the circulation applied to the annulus, $\Gamma = 2\omega \cdot \pi \bar{R}^2$:

$$\Delta\phi_{\rm rot} = \frac{\Gamma}{\kappa_o} \cdot 2\pi \frac{\mathscr{R}}{(1+\mathscr{R})} \tag{2.20}$$

As will be shown in Sec. IV, this is also the periodicity of the staircase pattern for each wound quanta of circulation, Eq. (4.8). Thus, the staircase pattern is periodic in the applied circulation, with period κ_o.

The annulus behaves similarly to an electronic circuit: a voltage source, V, with finite output impedance Z_o and series load Z_l. In this analog, the aperture is analogous to an applied load impedance, and the annulus hydrodynamic inductance is analogous to the voltage source output impedance. For the electrical case the voltage measured across the load is $V \cdot Z_l/(Z_l + Z_o)$. If the load impedance is large compared to the source impedance, then the voltage developed across Z_l is V. But if the load impedance is too small, $Z_l < Z_o$, then the voltage is diminished by the voltage division. A similar situation occurs with the superfluid annulus, where a constant phase develops across the aperture, $\Delta\phi_{\rm rot}$ if $L_a > L_{an}$. If this condition is not met, then the phase developed drops by the same voltage division form. The annulus is a "constant phase source" with an "output impedance" of L_{an}.[24]

III. CRITICAL VELOCITIES AND VORTEX NUCLEATION

If $v_{\rm rot}$ could be detected, one would have a sensitive gyroscope. Thus, the experimental question is: How can one detect this rotationally induced velocity through the aperture? A measurement of the critical velocity for vortex nucleation provides the means. After describing below the critical velocity and the physical process of vortex nucleation, we will explain how a diaphragm-aperture (D-A) oscillator is used to monitor the apparent vortex critical velocity in the aperture, and how this leads to a measurement of the rotationally induced phase difference.

It is important to understand the nature of the intrinsic critical velocity, since as will be shown, it ultimately determines the noise characteristics of a superfluid SQUID. Given below is a summary of the theoretical ideas used to describe and understand the critical velocity. We conclude with the current picture of quantized vortex nucleation and the definition of parameters used in this picture.[25]

It is observed that superfluid helium will flow with unmeasureable dissipation through narrow capillaries and channels up to some well defined velocity, v_c. Above this velocity, substantial dissipation is observed. Feynman first suggested in 1955,[26] that the onset of quantized vortex production could be responsible for this dissipation, and in 1961, Vinen considered the question of how the vortices can be created.[27] Vinen suggested that the vortices responsible for dissipation would nucleate preferentially on sharp features on the walls of a container and could be nucleated by thermal activation or quantum mechanical tunneling. His picture of vortex nucleation is the essence of the current theory describing vortex creation and critical velocity phenomena in apertures and porous powders.[28]

In 1966, Anderson showed, using quantum mechanical arguments, how vortex motion can lead to quantized dissipation in superflow. A vortex which crosses all the streamlines will decrease the superfluid phase difference across an aperture by 2π and decrement the velocity by:

$$\Delta v_{\text{slip}} = \frac{\kappa_o}{l_a} \tag{3.1}$$

where l_a is the hydrodynamic length of the aperture. This process of quantized dissipation in units of 2π phase drops, is called a 2π phase slip. This form of quantized dissipation is the mechanism by which the superfluid can change its circulation state and is similar to the dissipative transitions between quantized flux states in an RF SQUID.

Since the first detection of these phase slips,[8] there has been an effort to extract the vortex nucleation parameters directly from experiment.[29–32] In these sub-micron aperture experiments, it is observed that v_c is approximately a linear function of temperature:

$$v_c = v_{co}\left(1 - \frac{T}{T_o}\right) \tag{3.2}$$

where v_{co} is the zero temperature critical velocity and T_o is typically measured to be 2.0 K to 2.4 K. This dependence strongly suggests that the vortices responsible for the phase slips are thermally activated, and, can

be shown to be consistent with activation over a linear energy barrier: $E(v) = E_o(1 - (v/v_{co}))$.[29] This temperature dependence extends to ~ 200 mK where the critical velocity saturates.[33] This is thought to be the cross-over temperature where quantum nucleation is dominate.[34, 35] Experiments described here will be in the thermal nucleation regime.

What follows below are the theoretical definitions used in these models following Ref. 29. The parameters used for the thermal activation model are attempt frequency, Γ, and energy barrier, $E(v_s, T)$. The procedure for connecting these parameters to experiment is outlined below and uses the definitions in Ref. 32. The essence of the theory is thermal activation over a velocity dependent energy barrier. The rate of phase slips is given by the Arrhenius law,

$$\nu_{\text{slips}} = \Gamma e^{-E(v, T)/k_b T} = e^{-E^*(v, t)/k_b T} \tag{3.3}$$

where, $E^*(v, T) = E(v, T) - k_B T \ln \Gamma$. After a time, t, the probability to have at least one slip is:

$$P(t) = 1 - \exp\left\{ -\int_0^t \exp\left(-\frac{E^*(v(t), T)}{k_b T} \right) dt \right\} \tag{3.4}$$

For oscillating flow such as in the diaphragm-aperture oscillator type experiments, $v(t) = v_p \sin(\omega_H t)$, and the probability of having a phase slip in a half cycle is:

$$P_{1/2}(v_p) \approx 1 - \exp\left\{ -t_f \sqrt{\frac{2}{\pi c_2 v_p}} \exp\left(\frac{E^*(v_p, T)}{k_b T} \right) \right\} \tag{3.5}$$

where $t_f = (1/2\nu_H)$, and

$$c_2 = -\frac{1}{k_b T} \frac{\partial E^*}{\partial v}\bigg|_{v_c} \tag{3.6}$$

This probability is calculated by expanding the sin ωt. The probability distribution, $P_{1/2}(v_p)$, can be characterized by two parameters: v_c and Δv_{therm}. The critical velocity, v_c is defined such that $P_{1/2}(v_c) = \frac{1}{2}$. The statistical width of the probability distribution, Δv_{therm}, is defined by the inverse slope of $P_{1/2}(v)$ at $v = v_c$:

$$\Delta v_{\text{therm}} = \frac{1}{(\partial P(v)/\partial v)|_{v_c}} = \frac{2}{\ln 2} k_B T v_{co} \left(-\frac{\partial E^*}{\partial (v/v_{co})}\bigg|_{v_c} \right)^{-1} \tag{3.7}$$

where v_{c0} is the $T=0K$ critical velocity. If one approximates the probability distribution of phase slips with a Gaussian,[36] then

$$\sigma_{\text{therm}} \approx \frac{\Delta v_{\text{therm}}}{\sqrt{2\pi}} \tag{3.8}$$

This reveals the interpretation of Δv_{therm} as a measure of the distribution width of the phase slips.

IV. DIAPHRAGM-APERTURE OSCILLATOR TECHNIQUE

A. Diaphragm-Aperture Oscillators: Phase Slips and Staircase Patterns

The experimental device which allows one to detect and study the quantized dissipation is a diaphragm-aperture (D-A) oscillator of the type used by O. Avenel, E. Varoquaux and coworkers (AV).[37] The generic two hole, D-A oscillator, shown in Fig. 4, is formed from a box with two openings: a sub-micron aperture of hydrodynamic inductance L_a, combined in parallel with a fine tube of hydrodynamic inductance L_p. Both openings are of comparable hydrodynamic inductance. One wall of this box contains a flexible diaphragm with spring constant k_H.[38] Assuming the superfluid is incompressible, when the diaphragm moves, superfluid moves through the openings. The aperture, because of its small size, allows only

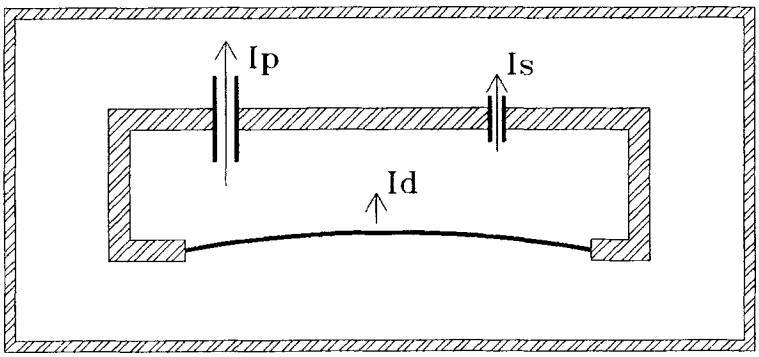

Fig. 4. Sketch of generic AV-type D-A oscillator showing directions of the mass currents through the aperture and the fine tube, which is generated by the flexible diaphragm.

a supercurrent v_a, while in the parallel channel, both the normal and super components are free to move with velocity v_p:[39]

$$I_D = I_a + I_p \tag{4.1}$$

$$\rho A_D v_D = \rho_s a_a v_a + \rho a_p v_p \tag{4.2}$$

where I_D, I_a, I_p are the mass currents displaced by the diaphragm, aperture, and parallel channel, and A_D is the effective area of the flexible diaphragm. If we take the circulation integral around a loop threading the aperture and parallel tube, we have from the quantization of circulation, Eq. (1.2):

$$v_p l_p - v_a l_a = n\kappa_o \tag{4.3}$$

This describes how trapped, quantized circulation divides between the two holes. Combining the last two equations, we can relate the diaphragm velocity to the superfluid velocity in the aperture and the circulation state of the two holes, n:

$$V_D = \frac{\rho_s}{\rho}\frac{a_a}{A_D}(1+\mathscr{R})\, v_s + \frac{a_p}{l_p}\frac{\kappa_o}{A_D} n \tag{4.4}$$

where we have defined the aperture and parallel channel hydrodynamic inductances to be:

$$L_a = \frac{l_a}{\rho_s a_a} \qquad L_p = \frac{l_p}{\rho a_p} \tag{4.5}$$

and

$$\mathscr{R} = \frac{L_a}{L_p} \tag{4.6}$$

Notice that with the diaphragm at rest, $V_D = 0$, the velocity through the aperture for each quanta of circulation is:

$$v_a = \frac{\mathscr{R}}{1+\mathscr{R}}\frac{\kappa_o}{l_a} \tag{4.7}$$

which will produce a phase drop of:

$$\Delta\phi = 2\pi \frac{\mathscr{R}}{\mathscr{R}+1} \tag{4.8}$$

Using these equations and Eq. (2.10) to relate the pressure which displaces the diaphragm to the acceleration of the fluid in the aperture and parallel channel, one finds that such a system will oscillate:

$$F = -k_H x_D = \Delta p A_D = \rho A_D L_a \frac{dI_a}{dt} \tag{4.9}$$

$$= \rho A_D \frac{L_a}{1+\mathscr{R}} \frac{dI_D}{dt} = \rho^2 A_D^2 \frac{L_a}{1+\mathscr{R}} \frac{d^2 x_D}{dt^2} \tag{4.10}$$

This is the equation of motion for a harmonic oscillator with angular frequency:

$$\omega_H = \sqrt{\frac{k_H}{\rho^2 A_D^2} \frac{(1+\mathscr{R})}{L_a}} \tag{4.11}$$

In practice, oscillators of this type have been realized with resonant frequencies ranging from a few hertz to 1000 Hz.[37,40] The diaphragm-oscillator resonance differs from a Helmholtz resonance in that the potential energy is stored in the displacement of a diaphragm instead of the compression of the resonating material (in this case He).

The quality factor of this oscillator is dominated by dissipation caused by heat flow. At a finite temperature, one will have some normal fraction of helium which carries all of the entropy of the fluid. If we assume that when the diaphragm moves and drives a current into or out of the cell, only the superfluid component moves, then the ratio of normal fluid to superfluid inside the cell must change. This change in normal fluid fraction is equivalent to a change in temperature and thus, for each swing of the diaphragm, driving fluid into (out of) the cell, the temperature of the interior of the cell is lowered (raised). This temperature difference is accompanied by a heat current and one can show[41] that this heat flow is responsible for the dissipation in our particular cell. Typically, we find that the quality factor, Q, is $\sim 20,000$ at 0.30 K, and falls in agreement with theory as $\sim T^{-5}$ as temperature is increased.

Individual phase slips were first detected in a D-A oscillator in 1985 by AV.[8] The method of detection, as indicated in Fig. 5, is to weakly drive the oscillator at the D-A resonance and record the amplitude of each half cycle. Eventually, as the amplitude of oscillation grows, the superfluid

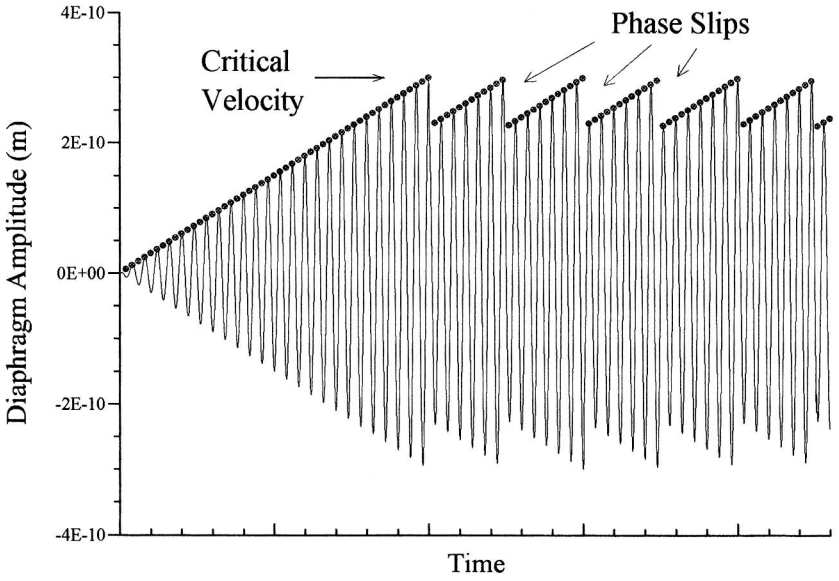

Fig. 5. Detection and effect of phase slips on resonantly driven Helmholtz oscillator.

velocity in the aperture reaches the critical velocity and a single vortex nucleates and crosses the flow in the aperture. The critical diaphragm oscillation amplitude when the superfluid velocity in the aperture is v_c, is:

$$X_D^c = \frac{\rho_s}{\rho}\frac{a_a}{A_D}\frac{(1+\mathscr{R})}{\omega_H} v_c + \frac{a_p}{l_p}\frac{\kappa_o}{\omega_H A_D} n \tag{4.12}$$

One can see that the diaphragm critical amplitude depends on the circulation state of the two holes. The circulation will have the effect of raising (lowering) the diaphragm critical amplitude for diaphragm motion that applies flow in the opposite (same) direction as the circulation. In fact, each quantum of circulation that is trapped between the two holes changes the critical amplitude by:

$$\Delta X_D^{\text{step}} = \frac{a_p}{l_p}\frac{\kappa_o}{\omega_H A_D} = \frac{1}{L_p}\frac{\kappa_o}{\rho\omega_H A_D} \tag{4.13}$$

The notation, ΔX_D^{step}, will become apparent when the staircase response is described. The relationship between superfluid velocity in the aperture, diaphragm amplitude, and circulation state is represented graphically in Fig. 6.

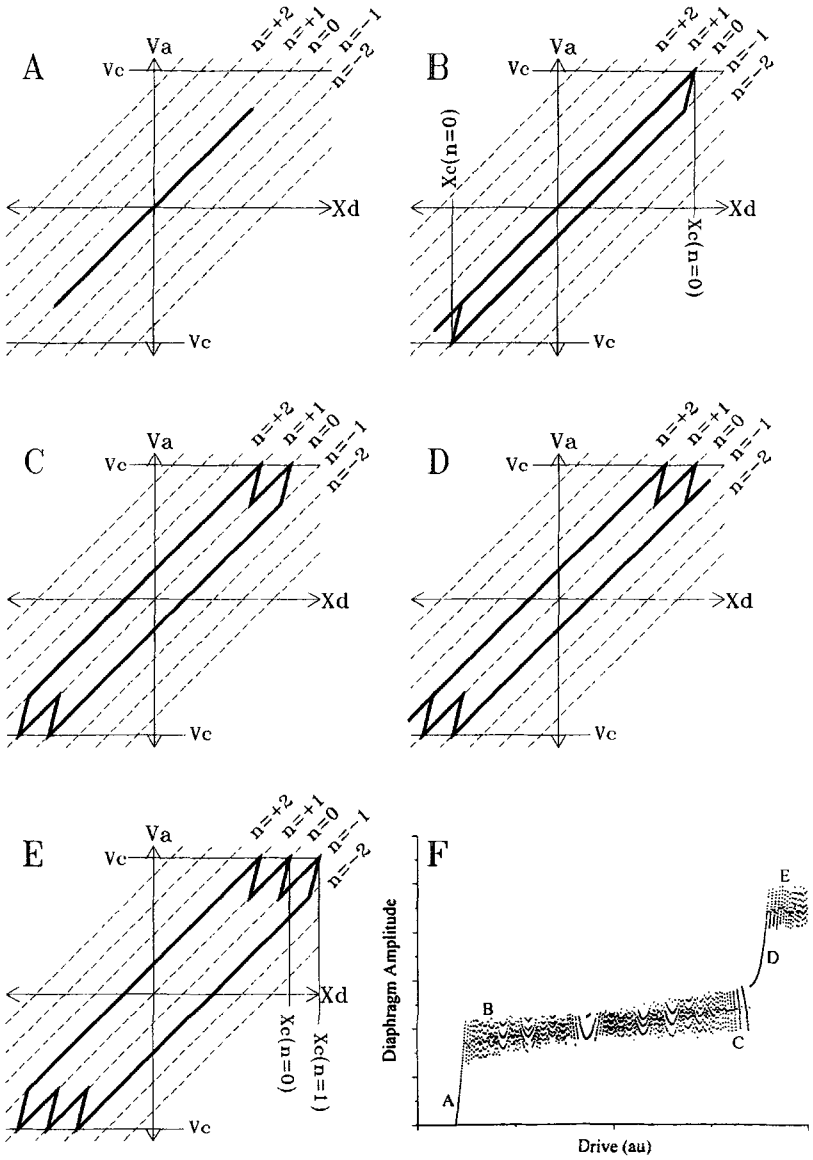

Fig. 6. Path of oscillator, shown as dark line, as a function of fluid velocity in aperture, Va, versus diaphragm amplitude, X_D, for various diaphragm drive power levels: A. Oscillator driven below critical amplitude; B. Phase slips at beginning of first step; C. End of first step, 4 phase slips per cycle; D. Riser leading to second step; E. Phase slips at second step. F. Simulated staircase showing positions of previous drive levels on staircase.

Figure 6A shows the oscillator in the $n=0$ circulation state, oscillating with amplitude less than the critical amplitude.

A useful definition to characterize an aperture is called the critical phase, which is defined to be the phase drop across the aperture at v_c, when $n=0$. Using Eq. (2.9) we calculate the critical phase $\Delta\phi_c$ to be:

$$\Delta\phi_c = 2\pi \frac{\rho\omega_H X_D^c A_D L_p}{\kappa_o(1+1/R)} \tag{4.14}$$

It is preferable to express $\Delta\phi_c$ in terms of the parallel channel inductance, L_p, since its dimensions are known to a higher precision as compared to the measurement of L_a from an SEM photo.

Each phase slip has three effects on the oscillator and flow field:[42]

1. A quantized reduction in superfluid velocity in the aperture:

$$\Delta v_{\text{slip}} = \frac{\kappa_o}{l_a}$$

2. A change in circulation state of the loop threading the aperture and parallel channel:

$$n \to n \pm 1 \text{where the sign is chosen such that the velocity in the aperture is reduced}$$

3. A loss of energy from the oscillator:

$$\Delta E \approx I_a \kappa_o \qquad \text{since typically} \quad v_c \gg \Delta v_{\text{slip}}$$

These changes produce a diaphragm amplitude decrement of:

$$\Delta X_D^{\text{slip}} = \frac{a_a}{l_a}\frac{\kappa_o}{\omega_H A_D} = \frac{1}{L_a}\frac{\kappa_o}{\rho\omega_H A_D} \tag{4.15}$$

Typically, $X_D^c \approx 100$ pm and $\Delta X_D^{\text{slip}} \approx 1$ pm (pm $= 10^{-12}$ meters). The circulation that is wound by a phase slip is in the direction opposed to the superflow in the aperture. Thus, on the next half cycle, the trapped circulation will lower the diaphragm critical amplitude. By comparing the change in diaphragm amplitude from a phase slip, to the change in critical diaphragm amplitude from the trapped circulation, one can see that:

$$\Delta X_D^{\text{slip}} < \Delta X_D^{\text{step}} \qquad \text{if} \quad \mathscr{R} > 1 \tag{4.16}$$

If this ratio of inductances is satisfied, the oscillator will experience another phase slip in the next half cycle. A D-A oscillator with $\mathscr{R} > 1$ has the

property that the phase slips come in pairs; the first slip winding a quanta of circulation which is then immediately unwound on the next half cycle. This has the effect of preparing the oscillator in the $n=0$ state for the next phase slip. These two consecutive transitions are shown in Fig. 6B. It should be understood that although only the transition history $n \to 0 \to -1 \to 0$ is shown, the transitions $n=0 \to +1 \to 0$ happen with equal probability. This is because the critical velocity for the two directions of diaphragm motion are degenerate. This degeneracy will be lifted by additional currents through the aperture from sources such as free vortices or rotation.

As the drive to the D-A oscillator as increased, the rate of the phase slips increases to absorb this power with the diaphragm oscillation amplitude saturated at X_D^c ($v_s = v_c$, $n=0$). This situation ends when there is enough power to drive the oscillator around the loop $n=+1 \to 0 \to -1 \to 0 \to +1$ each cycle of oscillation, as shown in Fig. 6C. As additional power is added, the diaphragm amplitude can now freely grow with the natural high Q response. This is shown in Fig. 6D as the small line segments growing along the $n=-1$ and $n=+1$ circulation states. The diaphragm amplitude stops increasing when the velocity in the aperture again reaches v_c for $n=-1$ and $n=+1$, and another phase slip is added to the dissipation loop shown in Fig. 6E. This new plateau, X_D^c ($v_s = v_c$, $n=1$), forms the second step a staircase pattern. As in the first step, the diaphragm amplitude saturates at this level until the power delivered to the oscillator is sufficient to drive a total of 8 phase slips per oscillation. This process forms a staircase pattern with step height given by Eq. (4.13) and the step length in power delivered to the cell given by:

$$P_{\text{step}} = 4\Delta E_{\text{slip}} \cdot v_H \approx 4\rho_s a_a v_c \kappa_o v_H \tag{4.17}$$

This dissipative process and staircase response curve is essentially identical to the behavior of a dissipative RF SQUID.[43]

Figure 6F shows the staircase generated by this dynamics. Shown are the peak amplitudes of each half-cycle of diaphragm oscillation which has been generated by a numerical simulation using a fourth order Runga–Kutta[44] to integrate the simple harmonic equation of motion for the diaphragm. Using Eq. (4.4), we can find the superfluid velocity at the aperture given the instantaneous diaphragm velocity and the circulation state threading the two holes. At each step in time, we calculate the probability for a phase slip at the aperture by using Eq. (3.3). We use a random number generator and create a phase slip event if this number is less than or equal to the probability for the slip. For each slip we decrement the supercurrent through the aperture and change the circulation state by one. Using this simple procedure, we can accurately replicate the recorded data (see Fig. 22).

Using these equations and Eq. (3.7) we can calculate an important performance characteristic of the superfluid oscillator, the step slope. As will be shown in Sec. V, this parameter is intimately related to the intrinsic circulation noise floor of this device and will determine its ultimate sensitivity as a gyroscope. At the beginning of the first step, the probability for a slip each half cycle is essentially zero. As the driving force is increased linearly, the probability of a phase slip also increases linearly in order to absorb the increasing power delivered to the oscillator. In the middle of the first step, the probability for the oscillator to make one dissipation loop is unity. Finally, at the end of the step, the probability for the oscillator to travel through two dissipation loops, is unity. Since the rate of slippage is an increasing function of superfluid velocity in the aperture, the average aperture velocity at the end of the step where the frequency of the slippage is ν_H is larger than at the beginning of the step where the frequency of slippage is near zero. This increase in aperture velocity, which is required to generate phase slips at higher rates, is also sensed as an increase in diaphragm amplitude. Because of this, it is expected that the step will have a nonzero slope. Using Eq. (4.12) and Eq. (3.7) we can calculate the slope of the step at X_D^c.

$$\frac{\Delta X_D^{\text{therm}}}{\Delta P_{1/2}} = \frac{\partial X_D}{\partial P_{1/2}(X_D)}\bigg|_{X_D^c} = \frac{\partial X_D}{\partial v_a}\frac{\partial v_a}{\partial P_{1/2}(v)}\bigg|_{v_c} \tag{4.18}$$

$$= \frac{a_a}{A_D}\frac{(1+\mathscr{R})}{\omega_H}\frac{1}{(\partial P_{1/2}/\partial v_a)|_{v_c}} = \frac{a_a}{A_D}\frac{(1+\mathscr{R})}{\omega_H}\Delta v_{\text{therm}} \tag{4.19}$$

Where in the above equations, $P_{1/2}$ is the probability for the oscillator to travel through one dissipation loop. Extrapolating this slope for half the step length, $\Delta P_{1/2} = 1$, we obtain the step rise:

$$\Delta X_D^{\text{therm}} = \frac{a_a(1+\mathscr{R})}{A_D\omega_H}\Delta v_{\text{therm}} \tag{4.20}$$

The figure of merit for the quality of the staircase pattern is this step rise, $\Delta X_D^{\text{therm}}$, compared to the step height, ΔX_D^{step}. Using Eq. (3.1), Eq. (4.13), and Eq. (3.7), we find:

$$\frac{\Delta X_D^{\text{step}}}{\Delta X_D^{\text{therm}}} = \frac{\mathscr{R}}{\mathscr{R}+1}\frac{\Delta v_{\text{slip}}}{\Delta v_{\text{therm}}} \tag{4.21}$$

$$= \frac{\mathscr{R}}{\mathscr{R}+1}\frac{\kappa_o}{l_a}\frac{\ln 2}{2k_B T v_{co}}\left(-\frac{\partial E^*}{\partial(v/v_{co})}\right)\bigg|_{v_c} \tag{4.22}$$

One can see that the rule of thumb is that the stochastic width, Δv_{therm}, should be less than the phase slip size, Δv_{slip} to realize a highly defined step pattern. Also, by measuring the step slope, we have a measure of the thermal activation parameter $(\partial E^*/\partial v)$.

B. Rotating Diaphragm-Aperture Oscillator

As we have shown in Sec. II, rotation can generate phase differences across an aperture. Here we will show how a phase difference has a measurable effect on the staircase response of a D-A oscillator. In the following section we will show specifically how our D-A oscillator design couples to rotation and produces a phase difference across the aperture similar to that in the ideal rotating annulus, Eq. (2.3). For the purpose of this discussion, assume that such a phase, $\Delta\phi_{\text{rot}}$, exists.

The v_{rot} which is produced by $\Delta\phi_{\text{rot}}$, will change the *apparent* critical velocity as measured by the diaphragm motion. If the critical velocity is measured with the device at rest, one will measure a critical diaphragm oscillation amplitude of ΔX_D^c and infer a critical velocity through the aperture of v_c. However, if one measures v_c while the device is rotating, the apparent critical velocity will change to $v_c \pm v_{\text{rot}}$, depending on the directions of applied flow and device rotation. For flow applied in the same direction of the rotationally induced current through the aperture, the apparent critical velocity will be lowered to $v_c - v_{\text{rot}}$, and like wise, for flow applied opposing the back flow, the apparent critical velocity will be raised to $v_c + v_{\text{rot}}$. The gyroscopic effect is sensed by detecting this shift in the apparent critical velocity.[45] The precise effect of $\Delta\phi_{\text{rot}}$ on the D-A oscillator response is given below, but the underlying physics is the simple velocity superposition that has been discussed here.

By inspecting a diagram of velocity through the aperture versus the diaphragm oscillation amplitude, as shown in Fig. 7, one can see the measurable effect on the D-A oscillator from a rotational phase difference. The broken diagonal lines in Fig. 7 show the relation between v_s and X_D when $\Delta\phi_{\text{rot}} = 0$. However, under rotation $\Delta\phi_{\text{rot}} \neq 0$, and there is an additional current bias through the aperture. This current will shift each circulation state as shown by the solid, diagonal lines in Fig. 7A. It is apparent from the figure that the diaphragm critical amplitude, represented by the intersection with the line at $v_a = v_c$, will no longer be degenerate for the two directions of flow. For the situation shown in Fig. 7, v_c will be reached at a lower diaphragm amplitude in the positive direction, while in the negative direction, v_c will be reached at a higher amplitude. Since the diaphragm motion is oscillatory, one always encounters the lowest critical amplitude and this results in a lowering of the first step. The diaphragm

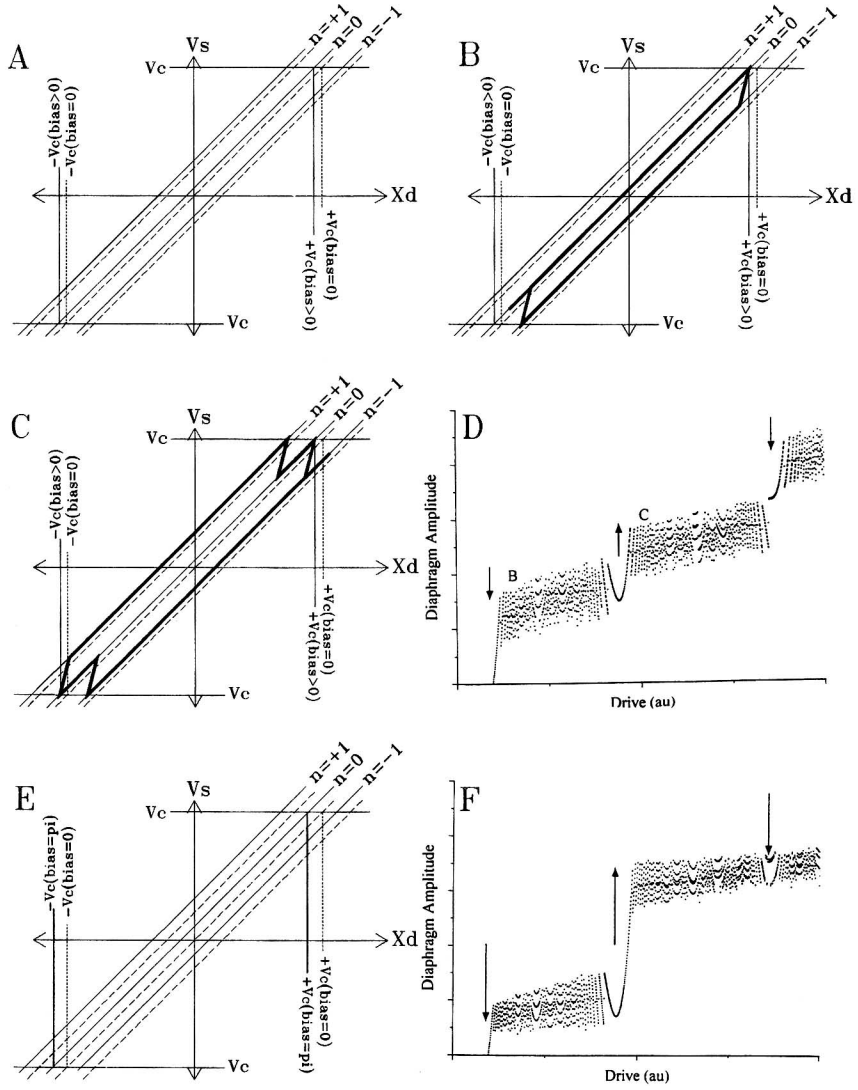

Fig. 7. Plot of fluid velocity in aperture, v_s, versus diaphragm oscillation amplitude, X_D. A. Shows shift of circulation states from rotational bias. B. Phase slips at lower diaphragm amplitude in + direction. C. Phase slips at higher diaphragm amplitude in − direction. D. Simulated staircase response. Arrows indicate motion of step from $\Delta\phi_{\text{tot}} = 0$ situation. E. Maximal rotational shift of circulation states. F. Simulated staircase response for maximum shift.

amplitude will saturate at this value, with phase slips only in the positive direction of flow, until the power delivered is sufficient to drive the oscillator around the path shown in Fig. 7C every cycle: 2 slips per cycle. Then, the diaphragm amplitude grows freely until it encounters the critical amplitude for the negative direction of flow. This effect is demonstrated in a numerically simulated staircase shown in Fig. 7D. The first half of the step is lowered and in this case is caused by phase slips generated for the positive direction of flow, while the second half of the step is raised and is a result of phase slips generated in the negative direction of flow.

This shift in the staircase will have a maximum when the bias is such that the shifted circulation states lie in the middle of the unbiased states. This corresponds to a rotational phase difference across the aperture of:

$$\Delta\phi_{\text{rot}} = \pi \frac{\mathscr{R}}{1+\mathscr{R}} \tag{4.23}$$

This state is shown in Fig. 7F. In this case, the first half-step is again caused by phase slips in the positive direction of flow in the $n=0$ circulation state. The second half of the first step which is generated by phase slips in the negative directions and $n=0$ circulation state, now meets the first half of the second step which is generated by phase slips in the positive direction of flow and the $n=-1$ circulation state. Thus, one observes the first step to be a lowered half step which is then followed by full steps. As more rotational flux is applied, the oscillator will reside in the $n=-1$ circulation state for small diaphragm motion. This state will have a smaller v_a, and thus a lower stored kinetic energy. Finally, when the phase difference

$$\Delta\phi_{\text{rot}} = 2\pi \frac{\mathscr{R}}{1+\mathscr{R}} \tag{4.24}$$

is reached, the circulation states have shifted by one full circulation quanta. The situation is now indistinguishable from the $\Delta\phi_{\text{rot}}=0$ case and the staircase pattern has its original shape.

Figure 8 shows the response of each circulation state to an applied rotational phase difference. If we drive the oscillator on any one step, and plot v_c versus ω, we expect a "triangle pattern" response. One can use this figure to find the various steps at a given rotational phase bias. This is done by drawing a vertical line at $\Delta\phi_{\text{rot}}$. The intersection of this line with the lines of each circulation states give the step locations.

The behavior of the steps is identical to the response of a dissipative RF SQUID to an applied magnetic field. The shifting of each circulation

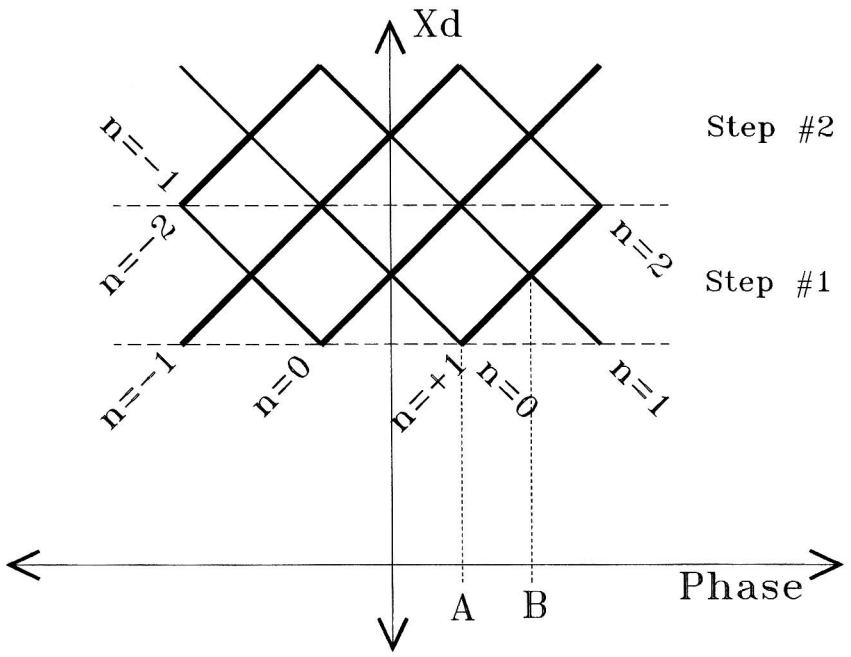

Fig. 8. Critical diaphragm amplitude versus rotational phase, $\Delta\phi_{\rm rot}$, showing triangle pattern. "A" marks maximum modulation at $\Delta\phi_{\rm rot} = \pi(\mathscr{R}/1 + \mathscr{R})$. At phase bias marked "B", the staircase is indistinguishable from $\Delta\phi_{\rm rot} = 0$.

state, which is demonstrated by the raising and lower of the steps, will provide the conclusive evidence for the rotational modulation. This particular response will distinguish the rotational effect from the less interesting suppression of the critical amplitude from other current sources, such as vibrationally driven currents through the aperture.

The superfluid SQUID is "read-out" in the same way as a superconducting SQUID, that is, one monitors the changes in the onset of dissipation to sense the rotation in the superfluid case, or magnetic field in the superconducting case.[46]

V. SUMMARY OF PHYSICAL CONDITIONS NECESSARY TO OBSERVE ROTATIONAL-MODULATION

In order to detect the shifts in the response of the D-A oscillator induced by rotation, one must first demonstrate the staircase response, one realize this response, one must minimize all environmental factors which affect the critical velocity in the aperture. Since there is no technique yet

developed to "flux lock" a superfluid SQUID, all sources of uncontrolled, fluctuating phase across the aperture must be significantly less than 2π for the time of measurement, which is typically a few hundred seconds. Sources of phase noise could be:

1. Random vortex motion in the cell.
2. Nyquist noise currents through the aperture.
3. Acoustically and vibrationally driven currents.

A. Thermal Environment

The temperature must be stable since the critical velocity and quality factor of the D-A oscillator are both strong functions of temperature. Above the quantum tunneling temperature of ~ 200 mK, the critical velocity follows closely:

$$v_c = v_{co}\left(1 - \frac{T}{T_o}\right) \tag{5.1}$$

where $T_o \approx 2$ K, and v_{co} is the extrapolated zero temperature critical velocity. The uncertainty in critical amplitude of the diaphragm from an uncertainty in temperature, σ_D^T, should be compared to the uncertainty in diaphragm critical amplitude generated by the distribution width of the individual phase slips. The uncertainty in diaphragm critical amplitude is:

$$\sigma_D^T = \frac{a_a}{A_D}\frac{1+\mathscr{R}}{\omega_H}\frac{\delta v_c}{\delta T}\delta T = \frac{a_a}{A_D}\frac{1+\mathscr{R}}{\omega_H}\frac{v_{co}}{T_o}\delta T \tag{5.2}$$

As will be shown, the uncertainty in diaphragm critical amplitude from the phase slip distribution after a measurement time, τ, is:

$$\sigma_D^{\text{slips}} = \frac{a_a}{A_D}\frac{1+\mathscr{R}}{\omega_H}\frac{\Delta v_{\text{therm}}}{\sqrt{2\pi\nu_H\tau}} \tag{5.3}$$

Thus for $\sigma_D^T < \sigma_D^{\text{slips}}$, we require:

$$\delta T < \frac{T_o}{\sqrt{2\tau\nu_H\tau}}\frac{\Delta v_{\text{therm}}}{v_{co}} = \begin{cases} 1.2\text{ mK} & \tau = 1\text{ min} \\ 160\ \mu\text{K} & \tau = 1\text{ hr} \\ 32\ \mu\text{K} & \tau = 1\text{ day} \end{cases} \tag{5.4}$$

This is not a difficult constraint for the measurement times of $\tau = 1$ min or $\tau = 1$ hour, and can be achieved with a properly designed thermal regulation

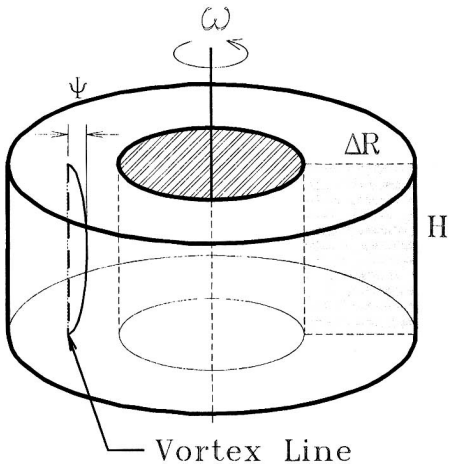

Fig. 9. Shows the deflection of a pinned vortex in a rotating annulus with septum on right.

system. However, for $\tau = 1$ *day* and even longer times, this constraint may become difficult to achieve. In this case, it may be advantageous to work in the quantum tunneling temperature regime ($T < 200$ mK) where the temperature dependence of the critical velocity is much weaker.

B. Motion of Free Vortices

Vortex motion is a serious problem, since (as shown below) a free vortex in the superfluid sample has the ability to produce a phase difference across the aperture of 0 to 2π. To demonstrate the effect of free vortices, we consider an annular container and a vortex positioned opposite the septum, with ends pinned to the lid and bottom, (see Fig. 9, septum at $\theta = 0$ and vortex at $\theta = \pi$). Figure 10 shows the calculated phase contours for this situation. As the vortex moves from the outer radius to the inner radius, the phase generated across the septum changes linearly from $\phi = 0$ to $\phi = 2\pi$. This is exactly the same situation as a phase slip in the microscopic aperture, although in this case the distance traveled is a macroscopic dimension of the container.

The uncertainty in the vortex position, σ_x, produces and uncertainty in phase difference across the aperture, σ_ϕ,

$$\sigma_\phi = \frac{2\pi}{\Delta R}\sigma_x \tag{5.5}$$

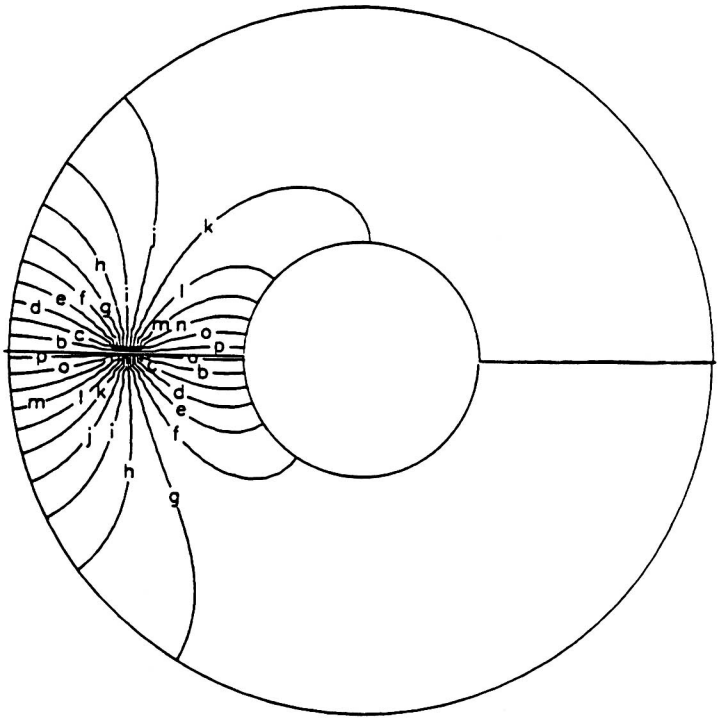

Fig. 10. Shows the calculated phase contours for a vortex positioned as in Fig. 9. Contours are space by 0.2 rads. In case shown, phase produced across septum on right side of annulus is $\sim\pi$.

where $\Delta R = R_{\text{out}} - R_{\text{in}}$. This uncertainty in phase difference can be represented as an equivalent circulation uncertainty, σ_Γ, using Eq. (2.20). Thus, the uncertainty in circulation generated by the uncertainty in vortex position is:

$$\sigma_\Gamma = \frac{\kappa_o}{\Delta R} \frac{1+\mathscr{R}}{\mathscr{R}} \sigma_x \tag{5.6}$$

This should be compared to the uncertainty in circulation caused by the finite width of the phase slip distribution (as shown in the next section in Eq. (6.4)). Using this one can estimate the amplitude of vortex motion that produces the same circulation uncertainty as the stochastic distribution of phase slips after a measurement time τ:

$$\sigma_x = \frac{\Delta v_{\text{therm}}}{\Delta v_{\text{slip}}} \frac{\Delta R}{\sqrt{2\pi \nu_H \tau}} = \begin{cases} 3.4\ \mu\text{m} & \tau = 1\ \text{min} \\ 430\ \text{nm} & \tau = 1\ \text{hr} \\ 88\ \text{nm} & \tau = 1\ \text{day} \end{cases} \tag{5.7}$$

where we have used $\Delta R = 1$ mm and $\Delta v_{\text{therm}}/\Delta v_{\text{slip}} = 0.5$. It is clear that a cell filled with a porous media would be desirable for long measurement times. We have not yet attempted to build a cell in this way.

Another possibility to minimize such motion is to use a ^{4}He sample mixed with ^{3}He. This permanent normal fluid provides dissipation for the motion of the vortex cores.[47] This normal fluid has the effect to lower the quality factor, Q, of the D-A oscillation. Typically we have tried concentrations of ^{3}He of about 0.1 % which gives a $Q \approx 200$. We did not observe any improvements using this mixture compared to nominal purity ^{4}He.

C. Brownian Motion and Nyquist Currents

Brownian motion of the D-A oscillator forces an interesting constraint on the hydrodynamic inductance.[48] The Equipartition Theorem states that every quadratic term of a system's total energy will have $\frac{1}{2}k_b T$ of thermal energy, (for $T \gg (\hbar\omega/k_b)$). The noise source which drives the system with this energy is the dissipative element of the oscillator. In the superfluid D-A oscillator case, the dissipation in the absence of phase slips is caused by heat flow from interior to exterior. It is the thermally driven fluctuations in the superfluid fraction of the fluid in the interior compared to the exterior, which will drive the oscillator to $\frac{1}{2}k_b T$ of thermal energy. This Nyquist noise supercurrent through the inductance of the aperture is found by equating:

$$E_{\text{therm}} = \tfrac{1}{2}k_b T = \tfrac{1}{2}L_a I_a^2 + \tfrac{1}{2}L_p I_p^2 = \tfrac{1}{2}L_a I_a^2(1 + \mathscr{R})$$

Using the connection between mass current I and phase $\Delta\phi$, we can calculate the phase noise across the aperture:

$$\Delta\phi_{\text{therm}} = \frac{2\pi}{\kappa_o}\sqrt{\frac{L_a k_b T}{1 + \mathscr{R}}}$$

As shown in Table I, thermal phase noise places a maximum on the hydrodynamic inductance of the aperture used; one can not use smaller and smaller apertures, without encountering increasing thermal phase noise.

TABLE I

Worst Case, $\mathscr{A} = 0$, Thermal Noise Across Aperture of Various Inductances at 0.3 K. Aperture Used in this Experiment is 1.0 μm x 0.19 μm

Aperture diameter	Inductance	Phase noise at 0.3 K
8 nm	$1.93 \cdot 10^5$ m^2/kg	$0.018\,\pi$ rads$_{rms}$
1.2 nm	$6 \cdot 10^6$	$0.1\,\pi$ rads$_{rms}$
12 pm	$6 \cdot 10^8$	π rads$_{rms}$

D. Vibrations and Acoustics

It is necessary to shield this device from vibrational rotations, such as pendulum modes of the apparatus. As shown above, a rotation will produce a phase across the aperture. Thus, to resolve the staircase pattern the phase noise produced by ω_{rms} must be less than 2π.

The oscillating pressure field from acoustic modes in the superfluid device can drive currents through the aperture, and thus, produce phase noise across the aperture. There are two possible sources of acoustic drive: sound which is external to the dewar, and the phase slips themselves which can drive the acoustic modes of the superfluid device. The first source of drive can be minimized by proper environment and acoustic shielding. This noise source was very detrimental to the larger volume cell experimented with at Berkeley,[9, 49, 35] but was found not to be an important problem for our microfabricated cells.

Data that is shown in Sec. VIII.A provides strong evidence suggesting that the phase slips can drive the acoustic modes and destroy the staircase response. If the aperture is at the end of an acoustic resonator, and acts as a fixed end, then at the aperture, the acoustic velocity field is 0, while the pressure will have amplitude $p(t) = p_o e^{i\omega t}$. Using the connection between mass current through the aperture and phase drop (Eq. (2.9)), and the relationship between pressure and mass current acceleration (Eq. (2.10)), we find the relationship between the phase produced across the aperture and the pressure amplitude of the acoustic mode with frequency ν:

$$\Delta\phi = \frac{p_o}{\kappa_o \nu \rho} \tag{5.8}$$

For the 1.5 kHz mode discussed in the following sections, $\Delta\phi = \pi$ when the pressure amplitude is 68 *mPa*.

In the experiments discussed here and in the experiments of O. Avenel and E. Varoquaux, the position detector used was a SQUID based system.

This position detection system relies on a steady, trapped current for sensitivity. This is as opposed to using a capacitance bridge position detector with a high amplitude, oscillating, excitation in the frequency range of kilohertz. It is possible for this excitation to drive acoustic modes of first sound in the superfluid container which could then drive oscillating superfluid currents through the aperture. Because of this possibility and high sensitivity, the SQUID based system is preferable.

Given that these constraints are met, one should observe a staircase response. This response, together with the proper geometry for rotational coupling, should allow one to detect rotationally induced phase differences.

VI. MINIMUM DETECTABLE ROTATION AND DEVICE LIMITATIONS

We can estimate the intrinsic sensitivity of this device as a gyroscope. The statistical width of the nucleation of the phase slip transitions determines this sensitivity. This width is related to the thermal activation parameters by Eq. (3.8). Using Eq. (4.12) we can relate the uncertainty in diaphragm amplitude, σ_D, to the uncertainty in nucleation velocity in the aperture for each phase slip, σ_a:

$$\sigma_D = \frac{a_a}{\omega_H A_D}(1+\mathscr{R})\,\sigma_a = \frac{a_a}{\omega_H A_D}(1+\mathscr{R})\,\frac{\Delta v_{\text{therm}}}{\sqrt{2\pi}} \tag{6.1}$$

After measuring N slips, where $N = \nu_H \tau$, the uncertainty in the diaphragm critical amplitude is:

$$\sigma_D(\tau) = \frac{\sigma_D}{\sqrt{\nu_H \tau}} \tag{6.2}$$

The modulation transfer function, that is, the meters change in diaphragm displacement for a circulation change in the gyroscope, is:

$$\frac{\Delta X_D}{\Gamma} = \frac{1}{L_p \rho_s \omega_H A_D} \tag{6.3}$$

Using this transfer function, we can calculate the circulation uncertainty:

$$\sigma_\Gamma = \frac{1}{\sqrt{\tau}}\sqrt{S_{\kappa_o}} = \frac{1}{\sqrt{\tau}} \cdot \frac{1}{\sqrt{2\pi}}\,\frac{1+\mathscr{R}}{\mathscr{R}}\,\frac{\Delta v_{\text{therm}}}{\Delta v_{\text{slip}}}\,\frac{\kappa_o}{\sqrt{\nu_H}} \tag{6.4}$$

where we have introduced the circulation spectral power density S_{κ_o} with a white power spectrum. This is valid under the assumption that the phase slips are uncorrolated.

Using Eq. (4.21) we can recognize the slope of the step in the above equation. Finally, we have an expression of the circulation noise spectral power density in terms of the step slope:

$$\sqrt{S_{\kappa_o}} = \left(\frac{\Delta X_D^{\text{therm}}}{\Delta X_D^{\text{step}}}\right) \frac{\kappa_o}{\sqrt{2\pi \nu_H}} \tag{6.5}$$

where for our device, $\sqrt{S_{\kappa_o}} = 0.030\, \kappa_o / \sqrt{\text{Hz}}$.

We can also express the noise spectral power density of the rotation resolution of the gyroscope expressed in units of $(\text{rads/sec})^2/\text{Hz}$. Since the circulation Γ is related to the rotation and area of the gyroscope by $\Gamma = \omega 2\pi R^2$, we have:

$$\sqrt{S_\omega} = \left(\frac{\Delta X_D^{\text{therm}}}{\Delta X_D^{\text{step}}}\right) \frac{\kappa_o}{2\pi R^2 \sqrt{2\pi \nu_H}} \tag{6.6}$$

For the device described in this work, the calculated sensitivity to a change in rotation state is: $\sqrt{S_\omega} \sim 15 \cdot 10^{-6}\ (\text{rad/sec})\ 1/(\sqrt{\text{Hz}})$.

One can see that this noise decreases as the operating frequency of the device is increased. In practice, this frequency will be limited by two constraints: diaphragm position detection, and driving acoustic modes in the superfluid. As the D-A frequency is increased, the critical amplitude decreases (Eq. (4.12)). The highest frequency allowed will be when the uncertainty from the position detector equals the uncertainty from the statistical distribution of the phase slips. Suppose the displacement sensor has a spectral noise density of $\sqrt{S_x}$. Then using Eq. (6.3), one has the uncertainty in circulation caused by the uncertainty in diaphragm position. For this uncertainty to be less than or equal to the uncertainty caused by the stochastic distribution of the phase slips we have the requirement on the position sensor:

$$\sqrt{S_x} \leqslant \frac{1+R}{(2\pi \nu_H)^{3/2}} \cdot \frac{a_a}{A_D} \Delta v_{\text{therm}} \tag{6.7}$$

For the parameters in the experiments reported here, $\sqrt{S_x} \leqslant 5 \cdot 10^{-13}$ $\text{m}/(\sqrt{\text{Hz}})$ and is more than satisfied with our typical position sensitivity of better than $5 \cdot 10^{-15}\ \text{m}/(\sqrt{\text{Hz}})$. This does show that the displacement sensing technology allows one to adequately sense oscillators with substantially

higher resonant frequencies, which, as shown above, would show lower circulation noise and thus higher sensitivity. In fact, with this level of position sensing, one could satisfy Eq. (6.7) with a maximum operating frequency of ~ 2 KHz.

As we will show in Sec. VIII, it is the possible for the phase slips to drive acoustic modes of the superfluid device. These acoustic fields can then drive uncontrolled supercurrents through the aperture, thus destroying the dynamics that generates a staircase response. There is a similar effect in the electrodynamic RF SQUID where the microwave modes can be excited.[50] This is a practical constraint and not a fundamental constraint, meaning that this coupling of the phase slips to the acoustic modes can be minimized by careful cell design.

Since more sensitive future gyroscopes are proposed to have large coiled sensing loops (see Sec. IX), it is interesting at this point to consider the fundamental constraints on the operating frequency and time response to a change in rotation rate. The D-A oscillator which is described earlier in this text, operates in the limit where the finite compressibility of the superfluid has a negligible effect. This will be the case if the operating frequency, ν_H, is much smaller than the lowest acoustical modes of the device. For the case of a D-A oscillator with a large coiled sensing coil of length l, this requirement is:

$$\nu_H \ll \frac{c}{l} \tag{6.8}$$

where c is the speed of first sound, ~ 240 m/sec. This will severely constrain the operating frequency of the largest D-A oscillator-based gyroscopes which have been proposed.[51]

However, Eq. (6.8) is *not* a fundamental requirement as there is no need to be limited to utilizing a D-A resonance. To sense the superfluid backflow generated by rotation, we need to monitor any resonance that couples supercurrents through the aperture. In principal, the acoustic modes of the large sensing loop could be driven, monitored, and used to sense the currents generated by rotation in the same way that the D-A resonance has been utilized. Also, as demonstrated in Sec. VIII, it is possible to modify the coupling between the aperture and the acoustic modes by aperture placement in the hydrodynamic circuit.

The fundamental temporal limits of a superfluid gyroscope break down into two questions: What is the maximum rate at which we can measure the critical velocity in the aperture? What is the time response of the superfluid sensing loop to a change in rotation? We address each issue as follows.

The time for a phase slip which is nucleated in a micron size aperture to complete its motion and consequently decrement the supercurrent is calculated to be $\approx 10\,\mu$sec.[52] Since this time is much longer than the sound propagation time through the aperture, $\approx 10^{-9}$ sec, the fluid in the aperture responds simply as an incompressible fluid. This suggests that the aperture can generate independent phase slip vortices at a rate of ≈ 100 KHz. However, this change in current will go unnoticed by the current sensing element, in this case a diaphragm, for a time comparable to the sound propagation time between the aperture and the diaphragm. For the device described in Sec. VII, this distance is at most about a centimeter. This gives a maximum frequency for the generation and detection of a staircase pattern of ~ 25 KHz, depending only on the distance between the aperture and the diaphragm.

The time for a superfluid gyroscope to respond to a change in rotation *is* limited by the sound time around the sensing loop. For the case of the ideal annulus, one can see from the analysis given in Sec. II that it is the motion of the septum that drives the superfluid in the annulus into motion $v_{ave} = \omega R$, and that it is the pressures created by the inertia of this accelerated fluid that drives the superfluid back-flow through the aperture. One can imagine to jerk the annulus, changing its rotation rate in a time short compared to the sound time around the annulus $\tau_{\text{jerk}} \ll 2\pi R/c$. This will launch two pressure fronts traveling away from the septum moving at the speed of first sound. The amount of fluid that has responded to the sudden change in septum velocity will grow linearly from 0 to the full value in a time of $\tau = \pi R/c$. Thus, we expect the backflow generated by this change of rotation to grow to its full value in a time comparable to the sound propagation time around the annulus $\tau = \pi R/c$. This delay produces a high frequency cut-off at a frequency of $\sim c/\pi R$. For the most extreme designs proposed to search for gravitational effects with sensing coils 400 m in length, this cut-off is at ~ 1 Hz. Reiterating, this is not a high frequency cut-off for the rate at which we can monitor the critical velocity, this is the highest frequency we expect the superfluid gyroscope to respond to rotation.

Interestingly, an expression analogous to Eq. (6.5) exists for the electrodynamic RF SQUID.[46, 53] In this case, one is interested in the flux noise spectral density:

$$\sqrt{S_{\phi_o}} = \frac{\sqrt{2\eta}}{\sqrt{\nu_{rf}}} \frac{\phi_o}{\sqrt{\text{Hz}}} \tag{6.9}$$

where $\eta = (\Delta X^{\text{therm}})/(\Delta X_D^{\text{step}})$ is the ratio of step rise to step height. The origins of Eq. (6.9) are very similar to the derivation of Eq. (6.5), that is,

thermal activation of quantized dissipation events over an energy barrier that decreases as the excitation increases. The excitation in the superfluid case is the velocity of the supercurrent in the aperture, where in the superconducting case it is the externally applied flux.[54, 55]

It is interesting at this point to compare the sensitivity of the superconducting RF SQUID to the analogous superfluid device. For the electrodynamic RF SQUID, typical values of η are, $\eta = 0.1 - 0.2$.[53] As we shall see, this value of η is not drastically different than the superfluid helium case where $\eta = 0.25 - 0.4$. However, in the superconducting case, $\nu_{rf} \sim 200$ MHz, where in the superfluid case $\nu_H = 66$ Hz. This difference in operating frequency contributes a factor of $\sqrt{(200 \cdot 10^6/66)} \approx 1700$ difference in spectral noise level. As mentioned, the operating frequencies of both superfluid and superconducting devices are limited by the excitations of fundamental self modes: kilohertz sound in the superfluid case and gigahertz microwave modes in the superconducting case. The dramatic difference in these frequencies is a consequence of the difference in the wave speed of each mode: the speed of light in the superconducting metal compared to the speed of sound in superfluid helium. Given this, for devices of similar size, we expect the superconducting device to operate at a frequency $(3 \cdot 10^8$ m/sec)/(240 m/sec) = $1.25 \cdot 10^6$ times higher than the superfluid oscillator, and therefore, to operate with a spectral noise floor $\sqrt{1.25 \cdot 10^6} \approx 1100$ times lower than the superfluid device.

VII. APPARATUS

Here we detail the apparatus including the design and construction of our D-A oscillators, the dc SQUID-based position sensor, and the necessary cryogenics and mechanics. We will show two miniaturized oscillator designs and discuss their performance in Sec. VIII.

A. Motivation for Device Layout

The miniature D-A oscillators were developed as a result of our previous experience with much larger D-A oscillators at Berkeley (volume $\approx 10\,\text{cm}^3$) and by the success of Avenel and Varoquaux (AV) with their miniature cell (volume $\approx 7\,\text{mm}^3$).[8, 56] Two oscillators constructed at Berkeley by Amar[9, 49] and by Davis[35] both showed single phase slips but never demonstrated a staircase response. Both larger oscillators showed extreme sensitivity to ambient acoustic noise: D-A oscillator mode driven by acoustics, suppression of the critical velocity, collapse of oscillator amplitude. Because of this, it was suspected that a smaller cell with intrinsically higher

frequency acoustic modes, might show lower sensitivity to the acoustic environment of the laboratory.

The idea for our particular device layout came primarily from two sources: the geometry of dc SQUIDs produced here at Berkeley by the Clarke group[46] and from the group in Trento, Italy[57] working with an annular container of superfluid. This device geometry was conceived as an attempt to combine the aesthetic appeal and calculable flow field of the ideal annular container with the proven D-A oscillators. It also bears resemblance to the fabrication of superconducting, thin film dc SQUIDs.

Figure 11A shows the relationship between our design and the superconducting dc SQUID. The superconducting SQUID is fabricated by

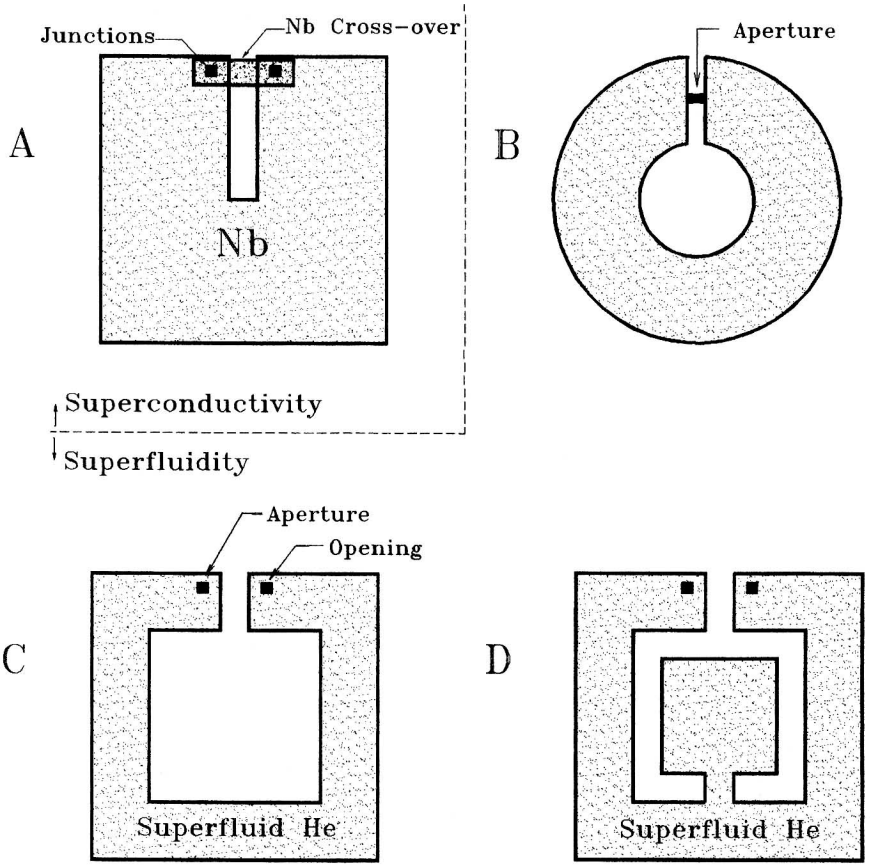

Fig. 11. Evolution of new cell from design of superconducting dc SQUID, A, and from annular container, B.

depositing a thin film of Nb. The Nb lattice "holds" the electronic superfluid and forms the container. This film is patterned to form a "C" shape by etching a slot. Then a film of Nb is used to cross the slot, making contact with the Nb below in two tunnel junctions (marked as black squares). The end result is an essentially two dimensional, annular container of superconducting electrons, with a septum. The septum is crossed by a film, making only weak contact to the bulk.

For the superfluid case, we must form a container since there is not a charged lattice to "hold" the fluid. Figure 11C shows the ideal superfluid container. In this case, we etch a flat cavity into a silicon wafer in the pattern shown. The cavity is closed by attaching a Kapton film to the raised surface. This forms a "thin" superfluid film which is analogous to the thin Nb film in the superconducting case. There must be a superfluid connection across the septum. This is provided by the holes etched into the silicon that penetrate the wafer. One of these holes is a large opening to the front side of the wafer, while the other is closed by a silicon nitride film with contains the sub-micron aperture. By embedding this device into a container of superfluid, we provide a continuous superfluid connection around the annulus.

In comparison to the Trento annular container, shown in cross-section in Fig. 11B, our device has two differences. The major difference is that our container forms a very flat annular volume. Since superfluid has a slip boundary condition at the top and bottom surfaces of the annular container, the height of the container is essentially irrelevant. The device in Trento, is an annulus with the height ≈ 10 mm and a diameter ≈ 24 mm. Our container has a similar size diameter, but is only 80 μm in height. Given the experience at Berkeley with large volume devices and the substantial improvement in performance with our miniature device, we felt that this could be a major design improvement to the annular containers. The second difference between our container and the Trento annulus is the location of the aperture. Our device routes the superfluid up and over the septum, where the Trento annular container has the aperture mounted directly in the septum. This difference is unimportant: as long as the hydrodynamic inductance of the aperture is significantly larger than the inductance of the annulus, then the phase difference across the septum will be unchanged, regardless of orientation.

Shown in Fig. 11D is a schematic of the realized design. We opened the center region to form a D-A resonator. The diaphragm is free to move over this center square, but is held rigidly over the sensing channel of the annulus by attaching a square silicon washer (described below). The D-A oscillator is necessary to provide a means to probe the critical velocity in the aperture. For a superconducting SQUID, this probe is accomplished by

external electronics. In the superfluid case, one must build the entire fluid circuit to sense the critical velocity, at low temperatures.

B. High Coupling, Planar Cell

The size of these oscillators was choosen such that we could utilize a natural source of low-noise rotation: the rotation of the Earth. This eliminates the technically difficult job of providing a low vibration rotation; one needs only to reorient the cell in the Earth's rotational field. This comes at the cost of the requirement to provide the cell with a low rotation noise environment. Rotation noise can come from sources such as the pendulum mode of the experimental probe, or from the tilting of a leaky air-spring.

Figure 12 shows design of D-A oscillator #1 (O1) and D-A oscillator #2 (O2) drawn to scale. This figure details the 80 μm deep relief on the back side of our 15 mm square, 0.5 mm thick, silicon substrate. Fabrication details of the silicon pieces is detailed in Appendix B. A flexible, 8 μm thick, Kapton sheet covers the entire back side of the chip. This sheet forms a thin slab container to hold the superfluid in the pattern shown in crosshatch, and forms the diaphragm element of the D-A oscillator. This

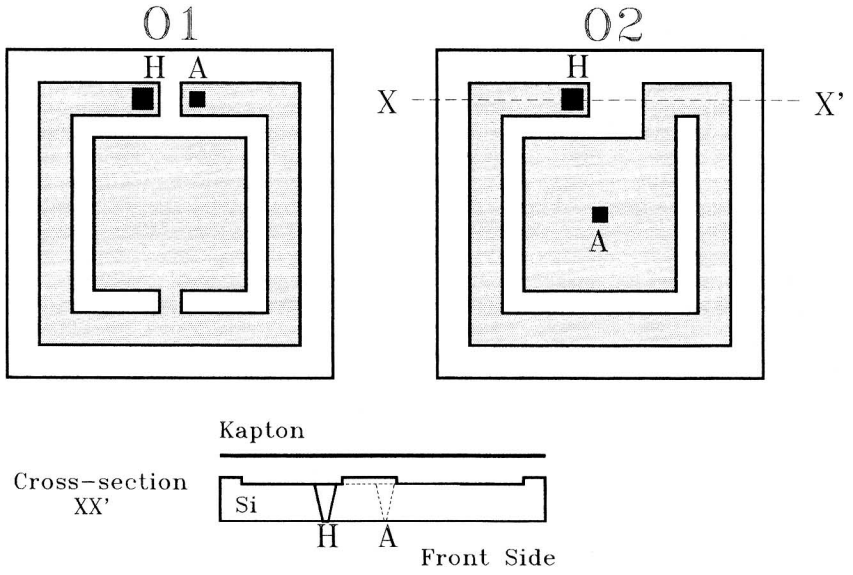

Fig. 12. Etch patterns for oscillators O1 and O2. Superfluid fills grey region, 80 μm thick. Aperture location is marked with "A" and parallel hole to front side is marked with "H".

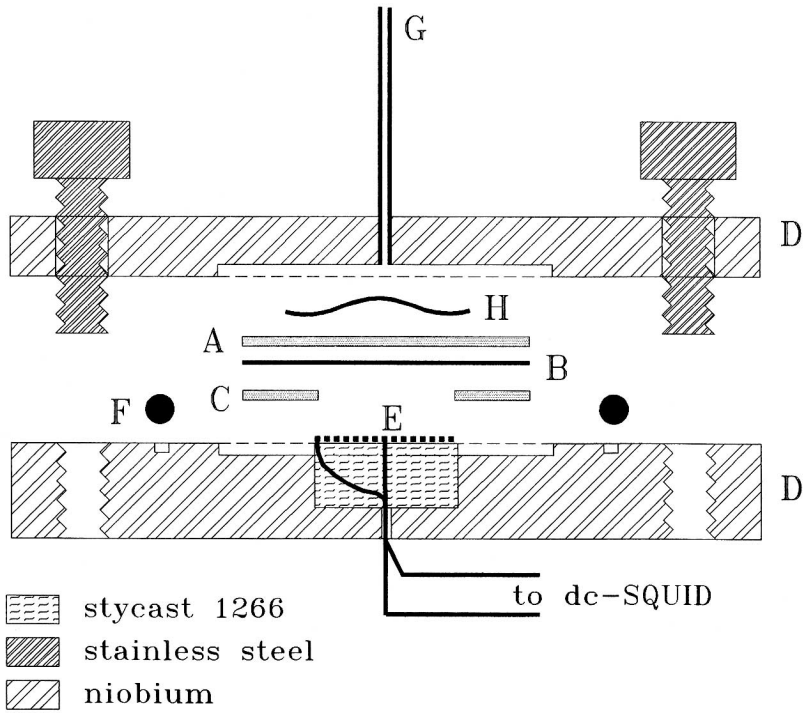

Fig. 13. Assembly of our D-A oscillator: A. superfluid D-A oscillator, B. Kapton diaphragm, C. silicon washer, D. niobium cell bottom and lid, E. superconducting displacement sensor, F. indium o-ring, G. fill tube, H. beryllium-copper spring.

container is surrounded by a close-fitting niobium box and is filled with superfluid, see Fig. 13.

The Kapton membrane is attached to the silicon cell with a thin film of Stycast 1266 epoxy. This membrane is attached on the side with the raised contours. The Kapton is patterned with a 100 nm thick aluminum film which serves as an electrode which is used to electrostatically drive the D-A oscillator by applying an oscillating voltage between the aluminum film and a gold electrode deposited on the cell.[58] On the side of the Kapton which will be external to the cell, we deposit a 200 nm thick film of niobium. This will serve as the superconducting plane for the displacement sensor.

The central square region, 7.0 mm × 7.0 mm, forms the flexible diaphragm member of a D-A oscillator, where the openings to the front side of the device, shown as black squares, form the openings of the two hole oscillator: one hole is located centrally over the diaphragm and terminates on a 100 nm thick SiN film on which is the aperture, while the

other hole is located at the end of the parallel channel and is 250 μm × 250 μm. The aperture is formed using electron beam lithography.[59] Notice in this design, there is no parallel fine tube as used in previous designs.[37, 60] Instead we create the proper parallel channel inductance which is necessary to generate a staircase pattern, by etching the flow path around the perimeter to the proper depth:

$$L_p = \frac{l_p}{\rho a_p} \tag{7.1}$$

where for O2 $l_p = 42$ mm is the channel length around the device, $a_p = wd$ is the cross sectional area of the channel, $w = 1.5$ mm. wide and 80 μm deep, and thus $L_p = 3.0 \cdot 10^3$ (m^2/kg). This was intended to form a $\mathscr{R} = 10$ D-A oscillator with an 200 nm × 1.0 μm aperture.

In order to hold the diaphragm rigid over the channel, we attach a silicon washer to the diaphragm when we epoxy the Kapton diaphragm to the cell. We use silicon to avoid any problems with relative thermal contraction. This washer is the size of the outer dimensions of the cell 15 mm, with a 7 mm hole etched completely through the 500 μm silicon substrate. This central hole allows the diaphragm to move freely in the center region and for the superconducting displacement transducer to penetrate the washer and approach the diaphragm.

This washer was found to be necessary. For our first iteration of this design, we did not use this washer. We found a dense spectrum of modes which were excited when the device was above v_c and phase slipping. These modes began at ~275 Hz and continued into the kilohertz range, and were not observed when the device was undriven or driven below v_c. When the washer was attached, the first mode which was observed, besides the D-A resonance, was the $\lambda/4$ acoustic resonance in the channel 1 KHz. These acoustic modes where also found to be problematic, see Sec. VIII.A.

This cell is then enclosed by a close fitting niobium box. The only openings to the superfluid bath surrounding the cell are through the aperture and larger etched opening of the parallel channel. By making the device holder itself from niobium, we have eliminated the need for any external superconducting shields surrounding the cell. We use 6.35 mm thick Nb plate for the bottom half of the cell holder which contains the electronic feed throughs and displacement transducer. We used 3.18 mm thick plate for the lid. We have had no problems with closing this cell leak tight and have found the niobium to be mechanically excellent (supports threads, stiff, etc.).

The diaphragm displacement sensor is a dc SQUID-based position sensor of the type used by the gravitational wave antennas[61] and is mounted

permanently in this niobium box. This has the important advantage that one can replace the silicon oscillator, without having to remake and reposition the displacement sensor. The sensor is a flat, spiral wound, coil of 50 μm diameter niobium wire: ~100 turns, 2 layers. Details of the displacement sensor are given below.

The assembled cell is attached to a homemade, one-shot, internally absorption pumped ^{3}He refrigerator. This refrigerator has a base temperature of 0.28 *K* and a run time of ~48 hours. We use an internal ^{4}He pot to condense the ^{3}He. We stop pumping the ^{4}He pot after condensation to minimize mechanical vibration. This refrigerator is placed on a vibration isolation stage with a resonance of ~1.5 Hz.

In order to make measurements with the apparatus oriented in various directions, we place the dewar on a rotating bearing. This bearing is constructed from two aluminum disks with ~4 *psi* of water injected between them. A central stainless steel pin keeps the two disks centered over each other. This allows the dewar to rotate with the top aluminum plate with sufficiently low mechanical vibration. A motor is used to smoothly reorient the dewar.

All electronic control and signals are routed through a low noise, miniature, 18 channel slip-ring. This slip-ring is mounted at the top of the refrigerator and allows for continuous measurement while smoothly reorienting the dewar.

C. Displacement Sensor

Here we report some considerations and experimental details about the dc SQUID-based position sensor. Careful design of this system is essential since it is sub-picometer diaphragm oscillations which are used to infer the superfluid current through the aperture.

The displacement transducer is a planner spiral coil, or "pancake coil." The transducer used in the earlier experiments described in Ref. 60 and Ref. 1 was simply 12 turns of 100 μm diameter superconducting wire, wound onto a brass stub.[62] This coil has an inductance of ~3 μH at room temperature and an estimated inductance of <0.2 μH when it is placed 50 μm from the superconducting diaphragm. This is a problem, as will be shown, since the input inductance to the dc SQUID used was 0.6 μH. Also, we observed a white noise floor which scaled as $\sqrt{T}$, where T is the temperature of the experiment. We suspected that we were detecting the Nyquist noise currents in the brass button. The solution of these two problems was straight forward: higher inductance transducer coil, and nonconducting substrate on which to wind the transducer coil.

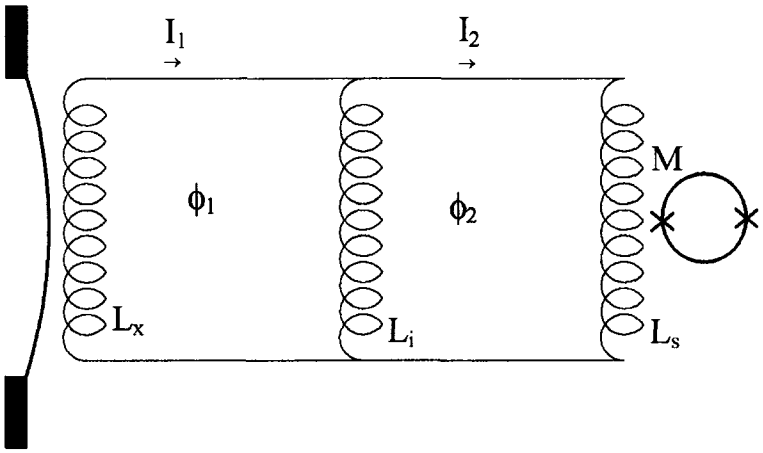

Fig. 14. Schematic of SQUID-based displacement sensor.

Figure 14 shows a circuit diagram of the displacement sensor.[61, 37] To understand the requirement on the transducer inductance we begin by writing the flux in each loop of the circuit.

$$\phi_1 = (L_x + L_i) I_1 - L_i I_2 \tag{7.2}$$

and

$$\phi_2 = (L_i + L_s) I_2 - L_i I_1 \tag{7.3}$$

where L_x is the inductance of the transducer coil, $L_s = 0.6\ \mu\text{H}$ is the input inductance of the dc SQUID, $L_i \approx 100\ \mu\text{H}$ is the inductance of the tank coil, $I_1 \approx 1$ A is the large current used to energize the transducer, and I_2 is the small signal current to the SQUID. This tank coil is used to shunt the large trapped current I_1, without this large current moving through the SQUID input coil. The inductance of the transducer is strongly affected by the close proximity to the superconducting film on the Kapton diaphragm:[63]

$$L_x = \mu_o n^2 a_c x \tag{7.4}$$

where μ_o is permeability of free space, n is the coil turn density, a_c is the coil area, and x is the distance to the superconducting plane. If the diaphragm moves, δx, the inductance of this coil will change, δL_x:

$$\frac{\delta x}{x} = \frac{\delta L_x}{L_x} \tag{7.5}$$

Since the flux in each superconducting loop remain fixed, there will be currents generated by this motion. We are interested in the signal current that is injected into the SQUID, δI_2:

$$\delta I_2 = -I_1 \frac{(\delta L_x/L_x)}{1+(L_s/L_i)+(L_s/L_x)} \tag{7.6}$$

Using the mutual inductance between the SQUID input coil and SQUID washer, $M = 10\,nH$, we can calculate the flux, $\delta\phi_{\text{squid}}$, that is generated by δI_2. One finds the displacement coupling, $(\delta\phi_{\text{squid}}/\delta x)$, to be:

$$\frac{\delta\phi_{\text{squid}}}{\delta x} = -\frac{MI_1}{x}\frac{1}{1+(L_s/L_i)+(L_s/L_x)} \tag{7.7}$$

Immediately, one can see two requirements to maximize the sensitivity: $(L_s/L_i) < 1$ and $(L_s/L_x) < 1$. The first requirement is met easily. In practice, we use a $L_i = 120\,\mu\text{H}$ coil: 4 layers of 125 μm diameter pure Nb wire, 60 turns per layer, 4 mm diameter. The transducer pancake coil used was: 2 layers of 50 μm diameter pure Nb wire (plus 25 μm of insulation), 5 mm diameter. We place this coil $\sim 100\,\mu\text{m}$ from the diaphragm which gives an average distance from the center of the windings to the diaphragm of $\sim 175\,\mu\text{m}$. This give an inductance of $L_x = 3\,\mu\text{H}$. The SQUID input inductance is $L_s = 1.87\,\mu\text{H}$, and thus the denominator of the last equation evaluates to $1+(L_s/L_i)+(L_s/L_x) = 1+0.02+0.61 = 1.63$. Using these parameters in Eq. (7.7), we should have a displacement coupling of:

$$\frac{\delta\phi_{\text{squid}}}{\delta x}\frac{1}{I_1} = 17\,\frac{\phi_o}{\text{nm}\cdot\text{A}} \tag{7.8}$$

where $\phi_o = 2.05\cdot 10^{-15}$ Wb is the superconducting flux quantum. In practice, we have realized 11 $\phi_o/(\text{nm}\cdot\text{A})$. This is a dramatic improvement of a factor of 30 in comparison to the coupling achieved with our previous sensor coils, where the coupling was 0.37 $\phi_o/(\text{nm}\cdot\text{A})$.

It is important to note that the inductance of the pancake coil drops as the gap, x, between the coil and diaphragm is reduced. Eventually, as the gap is reduced, the pancake coil inductance falls below the input inductance of the SQUID. At this point, no sensitivity gains are made by further reducing the gap. By replacing L_x in Eq. (7.7) with $L_x = \mu_o n^2 A x$ and taking the limit as $x \to 0$, one finds:

$$\lim_{x\to 0}\frac{\delta\phi_{\text{squid}}}{\delta x}\frac{1}{I_1} = \mu_o n^2 a_c \frac{M}{L_s} = 437\,\frac{\phi_o}{\text{nm}\cdot\text{A}} \tag{7.9}$$

where we have taken $L_s = 0.6\ \mu H$ which is the case for the Conductus dc SQUID used.[64] Note for the Quantum Design dc SQUIDs,[65] $L_s = 2\ \mu H$, and the maximum coupling in this case would be 131 $\phi_o/(\text{nm} \cdot \text{A})$.

We also made substantial improvements by proper choice of superconducting wire for the circuits other than the sensing coil. The previous circuit including tank coil and wires to the cell, was made with 125 μm diameter o.d., CuNi clad, 50 μm diameter NbTi core. In practice, we found it difficult to make high current superconducting joints since the core is only 50 μm diameter. In practice, we observed a critical current 0.26 A each cool-down, when the joint is made by pressing the wire to a bulk Nb pad with a #8 brass screw. We replaced all of this wiring with 125 μm diameter, pure Nb wire. We have also made Nb washers so that the wire

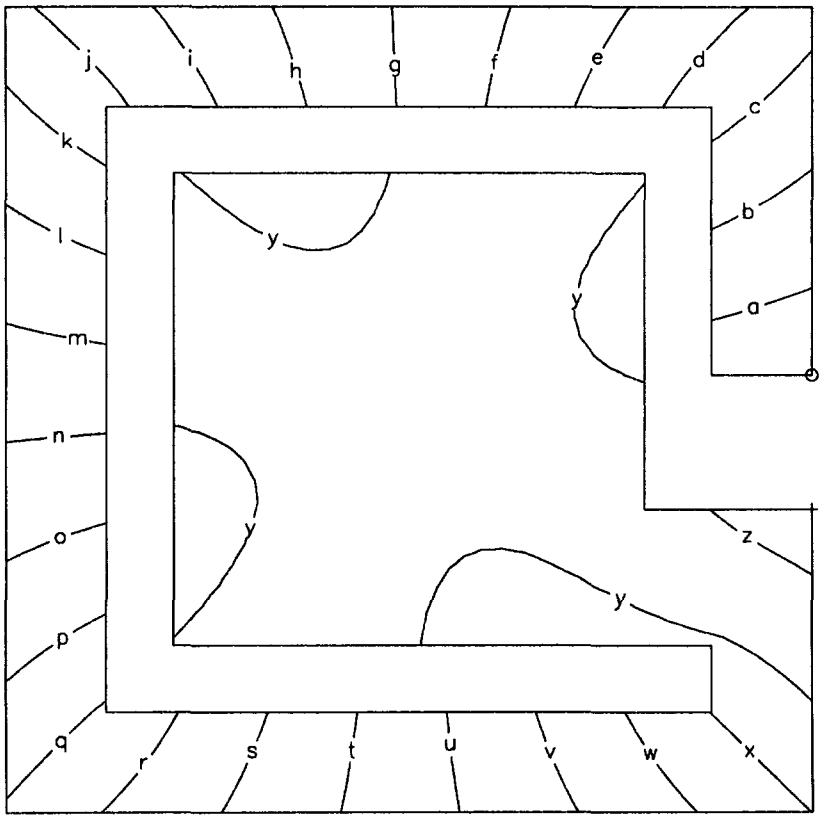

Fig. 15. Superfluid phase contours in cell rotating counter-clockwise with $\omega = 1$ (rad/sec). Contour levels are spaced by 500 rads.

is squeezed between two bulk Nb pads. With this larger diameter wire and Nb pads, we have increased the critical current to 1 A.

D. Rotational Coupling

This planar design has the significant feature that the superfluid flow field induced by rotating the container, is easily calculable. Figure 15 shows the calculated phase contours in oscillator O2 when the device is rotating with $\omega = 1$ (rad/sec) (solution for O1 is very similar). In this calculation we assume that there is no aperture. Figure 16 shows the superfluid velocity field viewed from the inertial frame, and Fig. 17 shows the velocity field

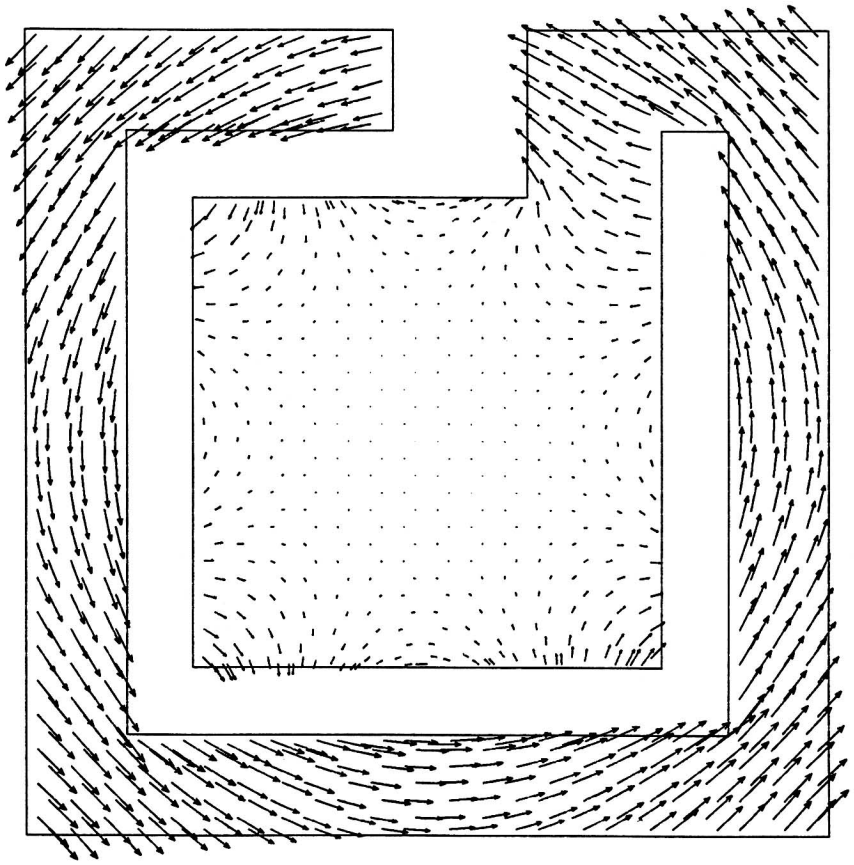

Fig. 16. Superfluid velocity field measured in the inertial frame when the cell is rotating with $\omega = 1$ (rad/sec).

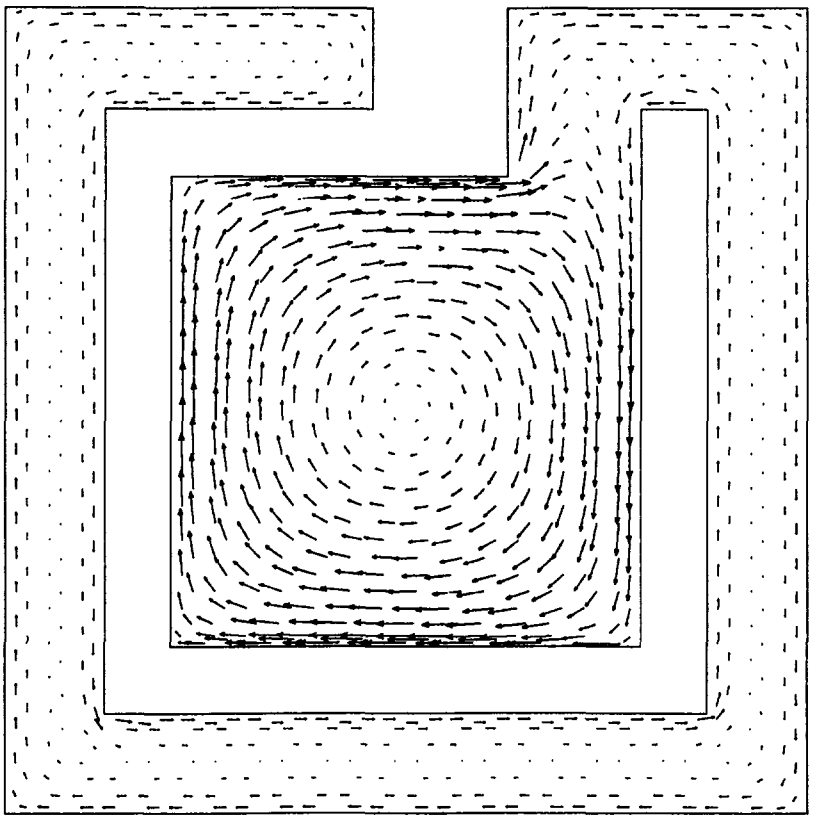

Fig. 17. Superfluid velocity field measured in the rotating frame when the cell is rotating with $\omega = 1$ (rad/sec).

measured in the rotating frame. The fluid in the perimeter channel has the same basic flow as that in the ideal annulus, (see Fig. 3); velocity $> \omega r$ for the inside radius, and velocity $< \omega r$ for the outside radius.

From the phase contours in Fig. 15 we see that the rotational coupling is

$$\frac{\Delta\phi_{\text{rot}}}{\omega} = 12.7 \cdot 10^3 \frac{\text{rads}}{\text{rads/sec}} = \frac{\pi}{247\ \mu(\text{rads/sec})} = 0.295 \frac{\pi}{\omega_E} \tag{7.10}$$

where $\omega_E = 72.9\ \mu(\text{rads/sec})$ is the angular velocity of the Earth. Using Eq. (2.3) which relates the phase produced to the rotation of an ideal annulus, we find that this coupling is equivalent to an annulus of average

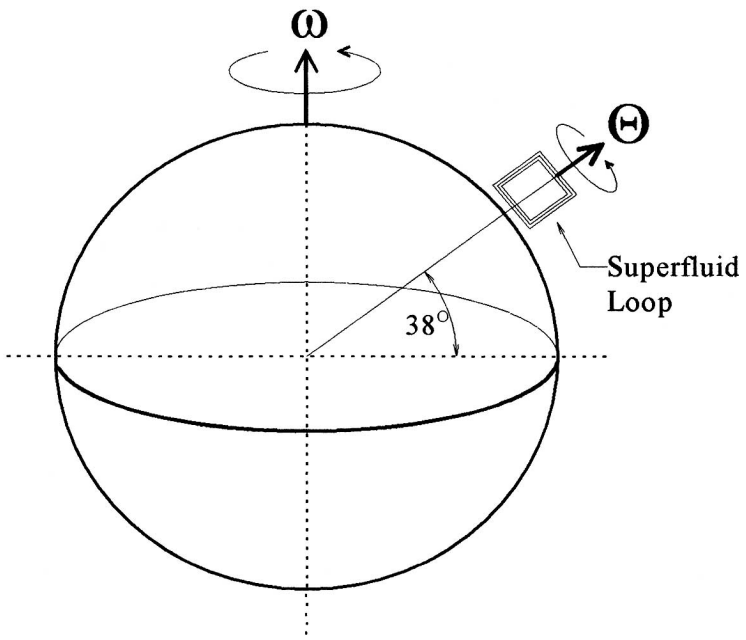

Fig. 18. Geometry to use Earth's rotation, ω, to modulated superfluid gyroscope. Orientation of sensing loop labeled as Θ.

radius, $R = 5.6$ mm. This ideal annulus has essentially the same "sensing area", A, as the rectangular container.

By reorienting the cell about the vector normal to the surface of the Earth, we can change the "projection" of the Earth's "rotational field" through the device. Figure 18 shows the device at the latitude of Berkeley, and in an orientation with none of the Earth's rotational flux penetrating the device. When the device is reoriented by $\pm 90°$, cell normal pointing north or south, the rotational flux will be $\pm \omega A \cos(38°)$, which will produce a phase $\pm 0.233\pi$. In this way we can modulate the apparent critical velocity of the device with the Earth's rotation.

VIII. EXPERIMENTAL RESULTS

Here we report the performance of two D-A oscillator designs, O1 and O2. Oscillator O1 was constructed first and failed to demonstrate the expected response for reasons which we detail below. As a result of our observations with oscillator O1, we designed and constructed oscillator O2. This design successfully demonstrated the superfluid gyroscope.

A. Performance of O1

Oscillator O1 demonstrated only a very weak staircase response. Figure 19 shows the measured response curve taken at 0.30 K with a nominally pure sample of ^{4}He and an aperture of size 1.0 μm × 0.30 μm. By subtracting a line from the portion of the response above the critical amplitude, we can resolve a very weak periodic response, shown in inset in Fig. 19. We experimented with a number of devices of this type and found this weak (or worse) performance as generic to this design.

We did notice an important signal which indicated the design flaw and failure mode of this device. We observed sound which was excited by the phase slips. These excited sound modes are consistent with the $\lambda/4$ and $\lambda/2$ modes of the sensing channel. Figure 20 shows two high frequency spectra of the diaphragm motioned one spectra with the cell driven below the critical amplitude and the other with the cell driven above the critical amplitude. When the cell is driven above the critical amplitude we find a mode at 1484 Hz. This is consistent with the $\lambda/4$ acoustic mode of the sensing channel; we predict 1460 Hz. We also see two strong modes excited a 2750 Hz and 3093 Hz. We predict the $\lambda/2$ mode at 2920 Hz. These modes can be

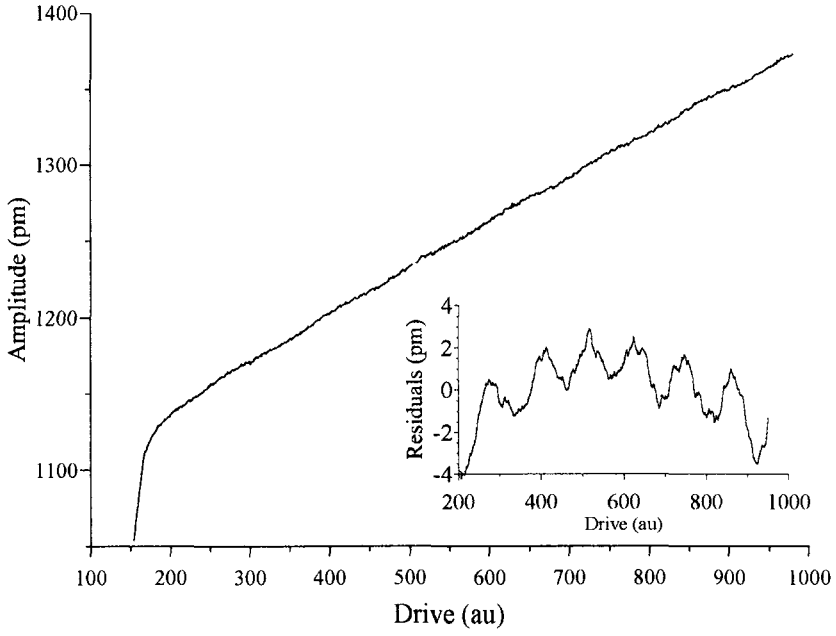

Fig. 19. Weak staircase response from oscillator O1. Inset graph is the residuals from a linear fit to response above critical amplitude.

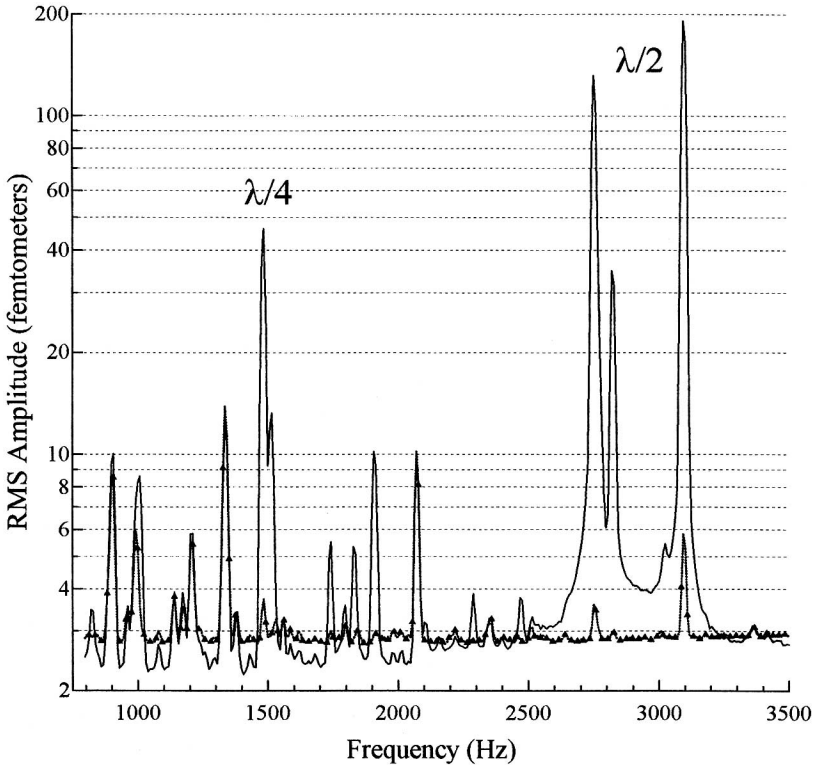

Fig. 20. High frequency diaphragm spectra comparing spectra with device O1 driven above and below the critical amplitude. Large peaks at 1484 Hz, 2750 Hz, and 3093 Hz appear when the device is driven above the critical amplitude.

driven by applying a resonant drive to the diaphragm and have a quality factor of $\sim 20,000$ at 0.3 K.

These modes are driven to an amplitude of from 50 fm to 150 fm above the noise floor of 1.5 fm.[66] It is possible that these modes could be the source of the uncontrolled current noise in the aperture which is responsible for destroying the expected staircase response. To estimate the amplitude of this acoustically driven phase noise across the aperture, we use a lumped circuit model,[51] where the diaphragm is a capacitive element, $C = (\rho^2 A^2 / k_H) = 2.75 \cdot 10^{-9}$ (Kg · sec^2/m^2), and the short neck, of length 1 mm and cross sectional area $80 \cdot 10^{-9}$ m^2, connecting the diaphragm to the sensing channel, is an inductive element, $L = 86$ (m^2/Kg), (see Fig. 12). These elements are in series. At $\nu = 3.0$ kHz the impedance of these elements are:

$$Z_C = 19\ \text{K}\Omega \qquad \text{and} \qquad Z_L = 1.6\ \text{M}\Omega \tag{8.1}$$

where Ω is the unit of hydrodynamic impedance which is defined to be the ratio of the superfluid mass current to driving chemical potential. One can see that all pressure drop will be across the inductive neck. Using a diaphragm displacement of 200 fm, we calculate a mass displacement at the diaphragm of $M = 1.42 \cdot 10^{-15}$ Kg, and a mass current of $I = 27 \cdot 10^{-12}$ Kg/sec. This will produce a pressure drop across the inductive neck of:

$$p = \rho L \omega I = 6.3 \text{ mPa} \tag{8.2}$$

Since we measure two modes at this frequency which are excited to this level, we will estimate the oscillating pressure to be ~ 10 mPa. This pressure field will drive currents through the aperture and produce a high frequency phase noise of amplitude:

$$\Delta\phi = \frac{p}{\kappa_o v \rho} = 0.23 \text{ rads} \tag{8.3}$$

which is substantial. This simple picture demonstrates that these phase slip driven acoustic modes have high enough amplitude to cause substantial phase noise across the aperture.[67]

These modes may be excited due to a poor choice of aperture location and hydrodynamic circuit. In this design, the aperture is at the end of the sensing channel which is a substantial hydrodynamic inductance. This inductance is in series with the aperture and is distributed over 20 mm. A phase slip produces a decrement of the mass current in both the aperture and the parallel channel. It is thought that a phase slip takes ~ 10 μsec to complete.[52] This time corresponds to a distance of 2.4 mm using the velocity of first sound, 240 m/sec. Since this distance is smaller than the length of the channel, sound must be produced; the end of the channel nearest the aperture has decelerated while the other end of the channel has not even received information that a slip has occurred. Because of this, we believe it to be important that the hydrodynamic circuit between the diaphragm and the aperture contain no substantial, spatially distributed, inductance.

Oscillator O2 was modified to avoid this excitation of acoustic modes by the phase slips. By moving the aperture directly over the diaphragm, the diaphragm acts as a "capacitive shunt" for the high frequency components of the pressure pulse generated by the sudden phase slip in the aperture. In this way, we weaken the coupling between the aperture and the kilohertz acoustic modes of the sensing channel.

B. Performance of O2

1. Phase Slips and Staircase Pattern

Our device has the sensitivity to resolve the underlying single phase slip dissipation events. Figure 21 shows the measured phase slips at 0.29 K with a sample of ^{4}He mixed with 0.1 % ^{3}He. The aperture is 1.0 μm × 0.19 μm in a 90 nm thick film of silicon nitride (from SEM photo). The cell has a resonant frequency of 66.5 Hz.

This measurement is performed by applying a resonant driving force between the electrodes deposited on the silicon cell and the Kapton diaphragm. We record the response of the oscillator amplitude as measured by the SQUID-based displacement sensor, with a lock-in amplifier. The drive amplitude is such that the rate of phase slips is ~ 0.1 Hz. This allows us to use a time constant on the output stage of the lock-in amplifier of ~ 0.1 sec.

The staircase response is measured by applying a linearly increasing resonant driving force, and recording the diaphragm oscillation amplitude. Figure 22 shows the measured staircase at 0.3 K with a sample of ^{4}He mixed with 0.1 % ^{3}He.

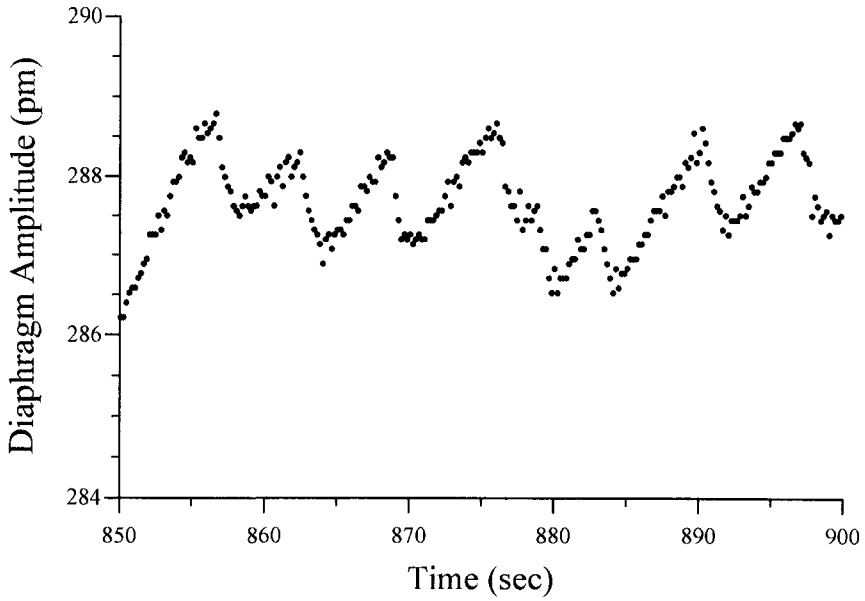

Fig. 21. Shows the response of the diaphragm while driving oscillator O2 to the critical amplitude. Quantized phase slips are evident by the sudden drops in oscillator amplitude.

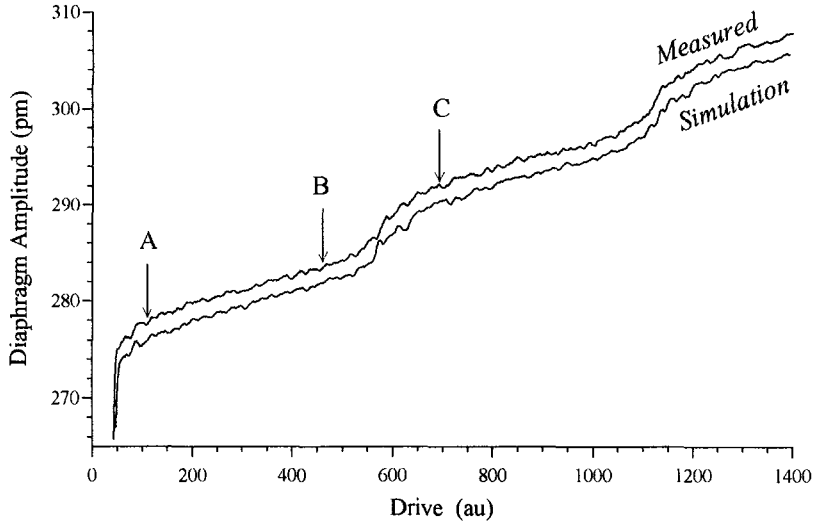

Fig. 22. Staircase response using oscillator design O2. Arrows shows where on response curve we drive to measure rotational modulation. Also shown is a computer simulation using the parameters given in the text (shifted down for visibility).

Plotted below the measured curve is a simulated staircase with parameters: $R = 7.5$, $X_D^c = 285.5$ pm, $\omega_H = 2\pi \cdot 66.5$ (rads/sec), $\delta v_{\text{slip}} = 0.40$ (m/sec), $\delta v_{\text{therm}} = 0.215$ (m/sec), $T_o = 2.11$ K, and $v_{co} = 11.9$ (m/sec). This parameter set is in accord with previous measurements of the phase slip critical velocity and nucleation parameters. In this case, $\delta v_{\text{therm}}/v_{co} = 0.018$ which matches well with previous measurements in other devices.[31, 68, 1] In this simulation rather than plotting the amplitude of each half-cycle as was done in Fig. 7, we simulate the signal processing of the lock-in amplifier.

2. *Modulation from the Earth's Rotation*

Given the size of the predicted coupling of this cell design to rotation, we used the Earth as a source of low noise rotation. Since the Earth's rotation is fixed, we reorient the sensing area of the cell and thus change the projection of the Earth's "rotational flux" through the sensing loop of the cell. Figure 18 shows the geometry used to sense the Earth's rotation. The cell is mounted with the normal to the sensing area in the horizontal plane. The cell is driven on the first step of the staircase. We then record the diaphragm critical amplitude as the cell is reoriented about the vertical axis of the dewar. We expect a sinusoidal variation of the projection of the rotation field onto the cell, and thus a sinusoidal variation of the rotational

phase difference, and finally a sinusoidal variation of the diaphragm critical amplitude.

As can be seen from the Fig. 18, the maximum expected projection of the Earth's rotation will be $\omega_E \cdot \cos(38°)$. This will apply a circulation flux to the gyroscope of $\Gamma_{\text{Earth}} = \pm 0.116\kappa_o$ as we reorient the dewar through 2π.

Because of the finite slope on the staircase pattern, it is necessary to use a numerical simulation to obtain the expected sensitivity to rotation. This is done by finding the set of cell parameters that produces a fit to the measured staircase. This fit is shown in Fig. 22.

Then, in the simulation, we modulate the staircase by adding a half quanta of trapped circulation. After doing this simulation, we expect our staircase to modulate by 2.7 pm for an applied circulation to the gyroscopes of $\kappa_o/2$. Thus, we expect a modulation of ± 0.63 pm measured at the diaphragm.

Figure 23 shows the results of this measurement. The cell was driven at the point on the staircase indicated by the arrow marked A, shown in Fig. 22. We reoriented the cell continuously at a rate of 1.0 rev/hour while recording ever 2 seconds the amplitude of diaphragm oscillation measured with a lock-in. As seen in Fig. 23, the critical amplitude has the expected

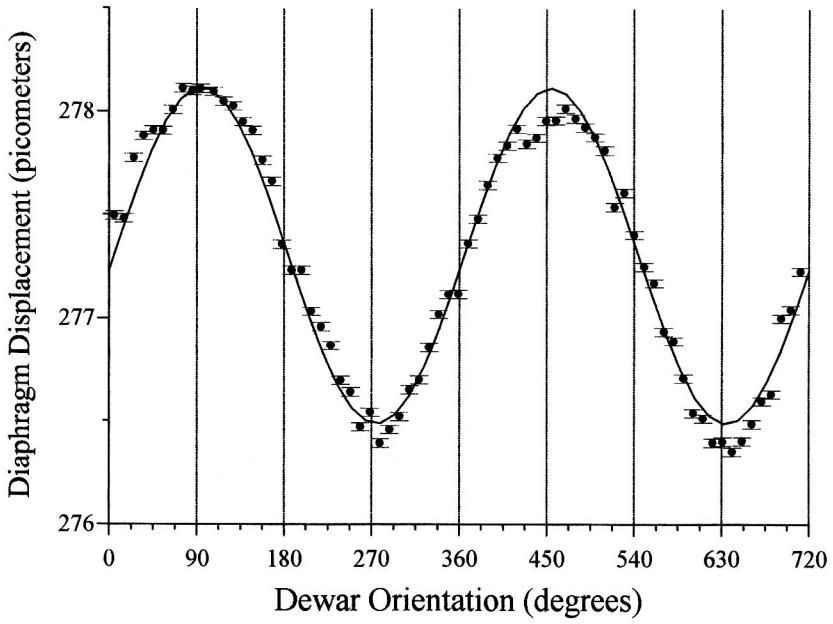

Fig. 23. Modulation of diaphragm critical amplitude from Earth's rotation shown with points and error bars. Best fit through data is shown as solid line.

sinusoidal variation as a function of dewar orientation. Each point plotted is a 120 second average. The error bars plotted are calculated by evaluating the standard error for each 120 second period. Typically, the error bars are 1.0% of the peak-to-peak modulation which agrees with expected noise calculation of Eq. (6.4), $\sigma/\Gamma_{\text{Earth}} = 1.2\%$. Also shown on Fig. 23 is a best fit through our data. This fit gives a modulation amplitude of ± 0.814 pm with a 90% confidence limit of ± 0.007 pm. At this time we do not understand the discrepancy between our measured and expected modulation.

The expected effect of the induced phase bias is that each step of the staircase will split in two: the first half of the step lowers while the second

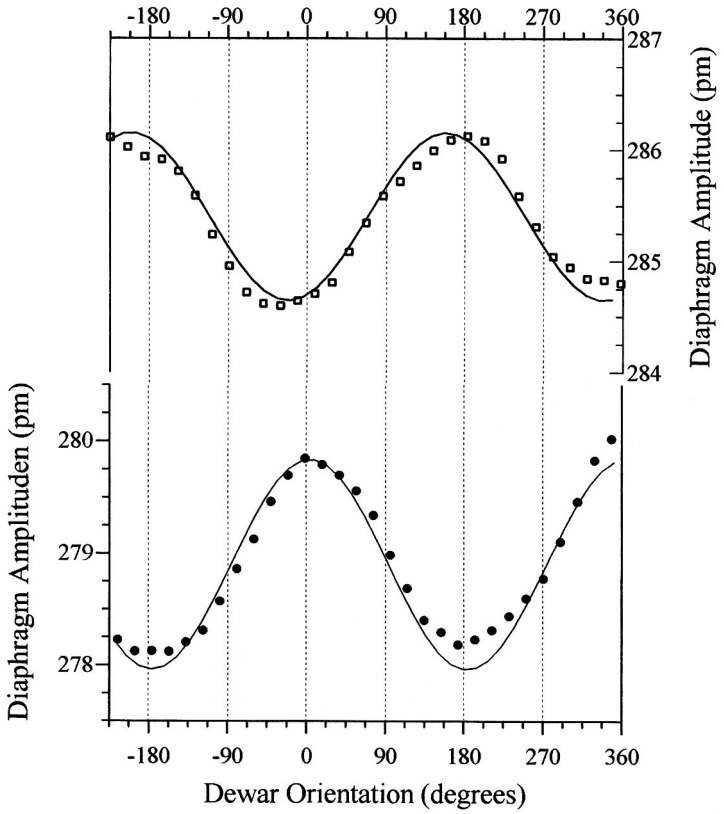

Fig. 24. Modulation of diaphragm critical amplitude from Earth's rotation measured at the beginning and at the end of the first step: triangle points are measured at a drive of 497 mV and plotted on left y-axis, while solid points are measured at a drive of 691 mV and plotted on right y-axis. Fits to each data set are shown as a solid, sinusoidal line. Note π phase difference between these two curves.

half of the step rises. In order to observe this, we programmed the computer to switch between two drive levels, the first drive level such that the oscillator is driven at the end of the first step, and the second drive level such that the oscillator is driven at the beginning of the second step (arrows marked B and C, shown in Fig. 22). We then recorded the amplitudes of these two levels while reorienting the dewar at a rate of once per hour. Figure 24 shows the measured response. This data shows that both locations on the staircase modulate with the applied rotational flux from the Earth, and that they modulate 180° out of phase, as expected.

This technique of chopping between two steps can be used to reject all spurious commonmode modulation signals that result from over-all shifts in the staircase pattern from sources such as temperature drifts of the cell. This technique may be very important for experiments which intend to average for extended periods of time ($\tau > 1$ day).

Figure 25 shows the measured noise spectrum in units of the circulation quantum per root hertz. The spectrum from 0.3 Hz to 3 mHz follows a power law, $\sqrt{S_{\kappa_0}} \propto f^{3/4}$. From Eq. (6.5) we expect a white noises spectrum of amplitude $\approx 15 \cdot 10^{-3} \kappa_0 / \sqrt{\text{Hz}}$. The origins of the measured excess noise are not yet understood. The most likely candidate is that of vortex motion within the device.

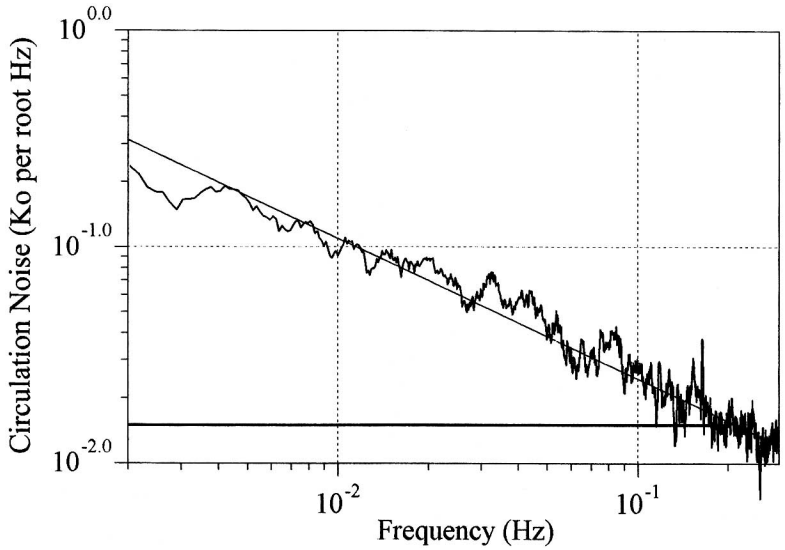

Fig. 25. Noise spectra of gyroscope in units of κ_0 per root hertz. Solid line shows the predicted white noise level.

One possible source of complication is from the fact that we continuously rotate the dewar to change the projection of the Earth's rotation. This rotation is at a rate which is 24 times greater than the signal that we intend to detect. Ideally, the rotation of the dewar does not couple to the cell since the sensing area is oriented perpendicular to this rotation. To check that a component of the rotation used to reorient the dewar does not project onto the cell, we monitored the diaphragm critical amplitude when the dewar was at rest and then immediately after beginning to rotate. We saw no measurable change in the diaphragm critical amplitude, and therefore conclude that any component of the reorienting rotation which projects onto the cell, must be small compared with the measured signal from the Earth's rotation.

IX. DISCUSSION: CONCLUSIONS AND DIRECTIONS

A. Conclusions

These experiments have succeeded in demonstrating a working superfluid gyroscope which is a close analogue of the superconducting RF SQUID. This gyroscope demonstrates an understandable staircase response and is modulated as expected by the Earth's rotation and is proof-of-principle that might lead to a new ultra-sensitive gyroscope technology.

We have developed a fabrication and construction technique which is found to be very useful in the development of our superfluid gyroscope. Since the superfluid D-A oscillator is generated using batch silicon processing techniques, and is separate from the displacement transducer, we were able to generate and test devices rapidly. Also, the planar construction allows easy numerical calculation of the flow field under rotation and thus an accurate prediction of rotational coupling.

We have found the acoustic considerations are essential to creating a successful design. In oscillator O1, we observed the acoustic modes of the sensing channel which were driven by the pressure impulses created by the phase slips. This design showed only a very weak "staircase" response. These modes are driven to an amplitude that drives a current through the aperture. This back-action of the phase slips produces a high frequency ($\sim$1.5 kHz) phase noise of substantial amplitude compared to π. By simply moving the aperture to a position directly over the Kapton diaphragm, as in oscillator design O2, we created a device with a high-quality staircase response. In the simplest terms, with the aperture in this location, the diaphragm acts as a high frequency "capacitive" short across the aperture. This substantially weakens the coupling of the aperture to the acoustic modes of the sensing channel.

This problem of the phase slips driving the acoustic modes is analogous to the situation in an RF SQUID where one is limited by the microwave modes of the SQUID: "Operation of a SQUID at very high (microwave) frequencies will be complicated by resonant modes of the device itself."[50] Unfortunately, the superfluid SQUID has high Q acoustic modes in the kilohertz range.

Our working device, O2, shows excess low frequency noise above the predicted spectral density. Although the origins of this noise are not clear as of yet, we strongly suspect vortex motion in the superfluid sample. We are considering various methods of providing strong pinning sites in and around the cell which will inhibit the motion of free vorticity.

The superfluid gyroscope demonstrated by O. Avenel and E. Varoquaux does not show this excess noise for measurement times lasting many hours.[13] Although they have not reported a noise power spectrum, this behavior is substantially better than the low frequency noise reported in these experiments where sudden shifts in bias are not uncommon. We suspect that the difference arises from the extensive vibration isolation constructed by Avenel *et al.*[30] This suggests that the excess low frequency noise reported in this work is not intrinsic to the superfluid.

More generally, we have demonstrated a superfluid phase difference detector. In the experiments described here, we have generated and detected a rotation induced phase difference. This device can be used to detect other sources of superfluid phase. For example, it has been predicted that a phase difference can be induced in superfluid ^{4}He by a combination of strong electric and magnetic fields.[69]

Just as in a superconducting RF SQUID, it is expected that the modulation versus applied phase bias should form a triangle pattern.[70] Since the Earth's rotation produces only $\pm 0.25\pi$ phase difference, the cell must be rotated manually to reach higher phase differences. This a current experimental goal.

ACKNOWLEDGMENTS

We would like to acknowledge: the many helpful conversations with S. Backhaus, S. Davis, S. Vitale, and R. Dolesi; A. Amar, J. Steinhauer, and Yu. Mukharsky for significant contributions on earlier experiments; A. Loshak for microfabricating the aperture used in the device reported in the main section of this paper; Marc Hadley of the Berkeley Sensors and Actuators Group for his helpful fabrication advice. Finally, we would like to thank the referees who's suggestions substantially improved this manuscript. This work has been partially supported by the National Science Foundation and the Office of Naval Research.

APPENDIX A: FLOW FIELD INSIDE ROTATING ANNULUS

In this section we present some details about the superfluid flow field inside an annular container as shown in Fig. 1. Here we are concerned with the velocity field in the annulus when there is no aperture in the septum.

As the annulus rotates, the superfluid must move with the septum. The average velocity in the $\hat{\theta}$ direction, averaged along any radial line is $\omega\bar{R}$, where $\bar{R}=(R_{\text{in}}+R_{\text{out}})/2$. This result can be seen by making a Gaussian surface, S, in the container as shown in Fig. 1. Since the superfluid velocity is divergence free,

$$\int_S \vec{v}_s\cdot\vec{da}=0=H\cdot\int_{R_{\text{in}}}^{R_{\text{out}}}\omega r\,dr-H\cdot\int_{R_{\text{in}}}^{R_{\text{out}}}\vec{v}_s\cdot\hat{\theta}\,dr$$

$$=H\omega\,\frac{R_{\text{out}}^2-R_{\text{in}}^2}{2}-Hv_{ave}(R_{\text{out}}-R_{\text{in}}) \tag{A1}$$

Solving for v_s, we find:

$$v_{ave}=\omega\bar{R} \tag{A2}$$

Although the velocity averaged along any radial line is $v_{ave}=\omega\bar{R}$, superfluid cannot rotate exactly as a solid body, $\vec{v}=\omega r\hat{\theta}$, and satisfy $\nabla\times\vec{v}=0$, since for solid body rotation $\nabla\times\vec{v}=2\omega$.

The superfluid flow field can be expressed analytically at the position which is opposite the septum. If the septum is at $\theta=0$, then at position $\theta=\pi$, by symmetry, the velocity field will have only a $\hat{\theta}$ component. At this position it is possible to solve Laplace's equation analytically and the velocity is found to be:

$$\vec{v}_s(r)=\frac{1}{r}\cdot\frac{\omega\bar{R}\Delta R}{\ln(R_{\text{out}}/R_{\text{in}})}\,\hat{\theta} \tag{A3}$$

where $\bar{R}=(R_{\text{out}}+R_{\text{in}})/2$, and $\Delta R=R_{\text{out}}-R_{\text{in}}$. The form of the velocity field is $(1/r)$, which is similar to the flow field of a vortex. Using the numerically calculated flow field, we find that Eq. (A3) is an excellent approximation to the flow field in the entire container. For the specific case of the geometry of the Trento annulus[21] the moment of inertia of the fluid calculated by assuming a simple $(1/r)$ velocity field produces only a 0.6% error compared to the moment of inertia calculated from the "exact" computer calculated velocity field. For comparison, if one approximated the flow field as a solid body with $v_s=\omega\bar{R}$, one would over estimate the moment of inertia by 25%.

APPENDIX B: DEVICE FABRICATION

This cell is microfabricated from silicon using a variety of techniques including photolithography, silicon micromachining, and electron beam lithography. This procedure is carried out entirely at the Berkeley Microfabrication Laboratory. These cells have two depths of bulk silicon etching: a 500 μm deep etch through the entire wafer to create the membrane which supports the aperture and a ~ 80 μm deep etch to create the superfluid cavity and flow paths. This has the problem that the fabrication cannot easily be done in the simplest flow: photolithography, nitride etching, silicon etching, then second layer of photolithography, nitride etching, and silicon etching. The problem is simply that the second layer of photoresist cannot spread over the silicon after the surface has been etched with grooves that are 500 μm or even 20 μm deep. This is because the photoresist is ~ 3 μm thick, which is thin compared to the surface features that are etched into the silicon.

This problem is solved by a procedure where one transfers all the patterning information into the silicon nitride film. Figure 26 shows the steps involved in this process. First let us remember the goal: deep etches in various locations to form the silicon nitride membranes and break lines to separate individual devices from the wafer; relatively shallow 80 μm etches for flow paths and D-A oscillator cavity; silicon nitride membrane 100 nm thick.

The process begins with a deposition of 200 nm of low stress silicon nitride, Fig. 26A. Then we spread photoresist over the front and back side of the wafer. Using a contact mask aligned we expose the pattern where the silicon will be etched completely through the wafer. We then etch the silicon nitride in this pattern completely to the bare silicon, Fig. 26B. We strip the wafer of the photoresist and respin another layer of photoresist. Now we expose the pattern where we will make the shallow etching of the silicon. We then carefully plasma etch the nitride thickness to ~ 40 nm, Fig. 26C. This etch is done in a few small steps. Each time we stop, we measure the thickness[71] and rotate the wafers. By measuring the progress in this manner, we can calibrate the plasma etch rate. By rotating the wafers, we obtain maximum etch uniformity. Then the wafers are stripped of photoresist. We have created three thicknesses of silicon nitride: 0 nm where we will etch the silicon deepest, 40 nm thick where we will etch only 80 μm, and 200 nm where we will not etch the silicon. The thin layer of nitride (40 nm thick) will be used to mask the silicon for the deep etch, and will be removed to allow the shallow etching. The wafers are then etched in KOH, (1 Kg KOH, 2 Kg H_2O, 80° C, ~ 1(μm/sec)), to form the silicon nitride membranes, Fig. 26D. We then etch 50 nm of the silicon nitride in

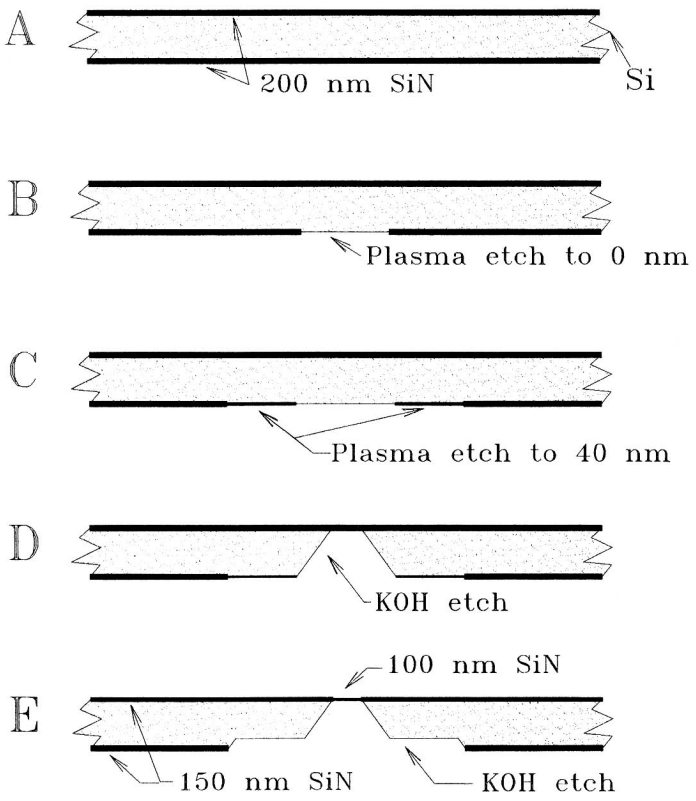

Fig. 26. Device processing. See text for description.

a concentrated HF bath. This is a wet process and the nitride is removed uniformly over the entire wafer. This has two effects: it removes the nitride over the silicon that must be etched only 80 μm, and it thins the membranes to 100 nm since it etches from the front and back side of the membrane. Then we etch the wafers again in KOH, to form the shallow features, Fig. 26E. This process removes the major difficulty in the previous fabrication recipe[60] and increases the yield up to this processing step to near 100%.

REFERENCES

1. K. Schwab, Ph.D. thesis, University of California, Berkeley (1996).
2. D. R. Tilley and J. Tilley, *Superfluidity and Superconductivity*, John Wiley and Sons, New York (1990).

3. D. D. Gregory and J. M. Goodkind, from unpublished research report.
4. J. R. W. Guernsey, in *Proceedings of the 12th International Conference on Low Temperature Physics*, E. Kanda, ed. (Keigaku Publishing Co., LTD., Tokyo, 1971), pp. 79–81.
5. M. Cerdonio and S. Vitale, *Phys. Rev. B* **29**, 481 (1984).
6. B. Crooker, Ph.D. thesis, Cornell University, Ithaca, NY (1984).
7. F. H. Wirth and J. W. Zimmermann, *Physica B* **107**, 579 (1981).
8. O. Avenel and E. Varoquaux, *Phys. Rev. Lett.* **55**, 2704 (1985).
9. A. Amar, Ph.D. thesis, University of California, Berkeley (1992).
10. J. C. Davis, unreported experiments with a two hole Helmholtz oscillator, Berkeley, 1992.
11. K. Schwab, N. Bruckner, and R. E. Packard, *Nature* **386**, 585 (1997).
12. O. Avenel and E. Varoquaux, *Czech. J. Phys.* **46**, 3319 (1996).
13. O. Avenel, P. Hakonen, and E. Varoquaux, *Phys. Rev. Lett.* **78**, 3602 (1997).
14. R. Hide and J. O. Dickey, *Science* **253**, 629 (1991).
15. J. Anandan, *Phys. Rev. Lett.* **47**, 463 (1981).
16. J. Anandan, *J. Phys. A* **17**, 1367 (1984).
17. For a comparison between a superfluid gyroscope and other experiments aimed at detecting the Lense-Thirring effect, see K. Schwab *et al.*, submitted to *JLTP* (Kharkov).
18. L. I. Schiff, *Phys. Rev. Lett.* **4**, 215 (1960).
19. Current state of the art rotation measurement is done with laboratory ring-laser gyroscopes and have a short term sensitivity of $6\,10^{-9}$ rads/sec per $\sqrt{\text{Hz}}$. However, drifts at the level of 10^{-6} rads/sec in a period of 1 hour have limited the long time measurements. See G. E. Stedman, Rep. Prog. in *Phys.* **60**, 615 (1997).
20. R. Dolesi, Ph.D. thesis, Universita degli Studi di Trento e Universita degli Studi di Padova, Trento, Italia (1996).
21. $R_{\text{out}} = 12$ mm, $R_{\text{in}} = 4$ mm, $H = 10$ mm.
22. PDEase, by Macsyma Inc. 20 Academy Street, Alington, MA 02174, USA.
23. The hydrodynamic length for a circular aperture of radius r in a wall of thickness l_o is: $l = (1/2)\,\pi r + l_o$ and for slot of height h and width w in a wall of thickness l_o, $l = (1/2)\,w \log(4h/w) + l_o$. See S. Burkhart, Ph.D. thesis, Universite de Paris-Sud, Centre d'Orsay, Paris, France (1995).
24. This calculation is in agreement with a previous calculation using a different perspective. See Ref. 57.
25. For reviews of this subject see: G. M. Schifflett and G. B. Hess, *J. Low Temp. Phys.* **98**, 591–629 (1995); Ref. 29; R. De Bruyn Ouboter, *et al.*, in *Progress in Low Temperature Physics*, C. J. Gorter, ed. (North Holland, Amsterdam, 1967), Vol. 5, pp. 44–78; V. P. Peshkov, in *Progress in Low Temperature Physics*, C. J. Gorter, ed. (North Holland, Amsterdam, 1964), Vol. 4, pp. 1–37.
26. R. P. Feynman, in *Progress in Low Temperature Physics*, C. J. Gorter, ed. (North Holland, Amsterdam, 1955), Vol. 1, pp. 17–53.
27. W. F. Vinen, in *Progress in Low Temperature Physics*, C. J. Gorter, ed. (North Holland, Amsterdam, 1961), Vol. 3, pp. 1–57.
28. J. S. Langer and J. D. Reppy, in *Progress in Low Temperature Physics*, C. J. Gorter, ed. (North Holland, Amsterdam, 1970), Vol. 6, pp. 1–35.
29. E. Varoquaux, J. W. Zimmermann, and O. Avenel, in *Excitations in Two and Three Dimensional Quantum Fluids*, A. Wyatt and H. Lauter, eds. (Plenum, New York, 1992), pp. 343–356.
30. O. Avenel, G. Ihas, and E. Varoquaux, *J. of Low Temp. Physics* **93**, 1031 (1993).
31. J. Steinhauer, K. Schwab, Y. Mukharsky, J. C. Davis, and Richard Packard, *Phys. Rev. Lett.* **74**, 5056 (1995).
32. J. Steinhauer, K. Schwab, Y. Mukharsky, J. C. Davis, and Richard Packard, *J. of Low Temperature Phys.* **100**, 281 (1995).
33. The behavior of the critical velocity in the low temperature limit is strongly effected by the concentration of ^{3}He. See Ref. 72, 73.
34. G. G. Ihas, O. Avenel, R. Aarts, R. Salmelin, and E. Varoquaux, *Phys. Rev. Lett.* **69**, 327 (1992).

35. J. C. Davis, J. Steinhauer, K. Schwab, Y. M. Mukharsky, A. Amar, Y. Sasari, and R. E. Packard, *Phys. Rev. Lett.* **69**, 323 (1992).
36. For a measured phase slip distribution and a Gaussian fit to this distribution, see: K. Schwab, J. Steinhauer, and R. E. Packard, *Phys. Rev. B* **55**, 8094 (1996).
37. O. Avenel and E. Varoquaux, in *Proceedings of the XIth International Cyrogenic Engineering Conference*, A. Wyatt and H. Lauter, eds., Butterworth, Guilford, England (1986), pp. 587–591.
38. The diaphragm spring constant is defined as $k_H = F/\delta x$ where F is the total force applied to the diaphragm and δx is the average diaphragm displacement.
39. Since our D-A oscillator has a $Q = \sim 4$ at $T > T_\lambda$, we infer that the parallel channel does not clamp the normal fluid.
40. B. Beecken and J. W. Zimmermann, *Phys. Rev. B* **35**, 74 (1987).
41. For a full calculation of this dissipative effect and comparison to measurement, see Backhaus, *Thermoviscous Effects in Steady and Oscillating Flow of an Isotropic Superfluid*, to be published (1997), or for a description of a similar calculation for the case of superfluid film flow, see J. E. Robinson, *Phys. Rev.* **82**, 440 (1961).
42. The exact expression for the energy drop is: $\Delta E = I_a \kappa_o (1 - (\Delta v_{slip}/2v_c))$.
43. J. E. Zimmerman, *J. App. Phys.* **41**, 1572 (1970).
44. W. Press, S. Teukolsky, W. Vetterling, and B. Flannery, *Numerical Recipes in Fortran: The Art of Scienctific Computing*, Cambridge University Press, Cambridge (1992).
45. To be precise, relative to the aperture, which is in the rotating frame, the superfluid velocity generated by rotation will be $v_{rot} + \omega r$. However, in the aperture, ωr is negligible in comparison to v_{rot} and for the purposes of this discussion will be ignored without any significant consequence.
46. J. Clarke, in *The New Superconducting Electronics*, H. Weinstock and R. W. Ralston, eds. (Kluwer Academic Publishers, The Netherlands, 1993).
47. R. J. Donnelly, *Quantized Vortices in Helium II*, Cambridge University Press, New York (1991).
48. Similar arguments are used to constrain the electronic inductance of the junction of a superconducting SQUID.[43].
49. A. Amar, Y. Sasaki, R. Lozes, J. C. Davis, and R. E. Packard, *Phys. Rev. Lett.* **68**, 2624 (1992).
50. J. E. Zimmerman, *J. App. Phys.* **42**, 4483 (1971).
51. R. Packard and S. Vitale, *Phys. Rev. B* **46**, 3540 (1992).
52. M. Bernard, S. Burkhart, O. Avenel, and E. Varoquaux, *Physica B* **194–196**, 499 (1994).
53. L. Jacket and R. Buhrman, *J. Low Temp. Phys.* **19**, 201 (1975).
54. J. Kurkijarvi, *Phys. Rev. B* **6**, 832 (1972).
55. J. Kurkijarvi, *J. App. Phys.* **44**, 3729 (1973).
56. O. Avenel and E. Varoquaux, *Phys. Rev. Lett.* **60**, 461 (1988).
57. M. Bonaldi, S. Vitale, and M. Cerdonio, *Phys. Rev. B* **42**, 9865 (1990).
58. We use Au since it has a low electrical resistance and can easily make contact to the Al film on the Kapton. A thin film of Cr 10 nm, is used to aid adhesion of the Au.
59. A. Amar, Y. Sasaki, R. Lozes, J. C. Davis, and R. E. Packard, *J. Vac. Sc. Tech. B* **11**, 259 (1993).
60. K. Schwab, J. Steinhauer, J. Davis, and R. Packard, *J. Microelectromech. Sys.* **5**, 180 (1996).
61. H. J. Paik, *J. App. Phys.* **47**, 1168 (1976).
62. Wire from Supercon: 50 μm NbTi core with 50 μm CuNi cladding and 25 μm insulation, total diameter of 125 μm.
63. H. A. Chan, M. V. Moody, and H. J. Paik, *Phys. Rev. D* **35**, 3572 (1987).
64. Conductus Incorporated, 969 West Maude Avenue, Sunnyvale, California 94086, Phone: (408) 523-9950.
65. Quantum Design, 11578 Sorrento Valley Road, San Diego, California 92121-1311 USA Telephone: 619.481.4400.
66. Bin size in FFT is 7.8 Hz and spectral density of displacement noise is $\sim 5 \cdot 10^{-16}$ $(m/\sqrt{Hz})$.

67. A more complete model of a similar situation has been calculated by Backhaus and will be published.
68. J. Steinhauer, Ph.D. thesis, University of California, Los Angeles, USA (1995).
69. H. Wei and R. Han, *Phys. Rev. Lett.* **75**, 2071 (1995).
70. S. Vitale, M. Cerdonio, and M. Bonaldi, *Physica B* **178**, 347 (1982).
71. We use a Nanospec/AFT thin film measuring device; Nanospec Inc., Sunnyvale, CA 94086.
72. G. Ihas, O. Avenel, and R. Aarts, *Physica B* **194–196**, 583 (1994).
73. Y. M. Mukharsky, K. Schwab, J. Steinhauer, A. Amar, Y. Sasaki, J. C. Davis, and R. E. Packard, *Physica B* **194–196**, 591 (1994).